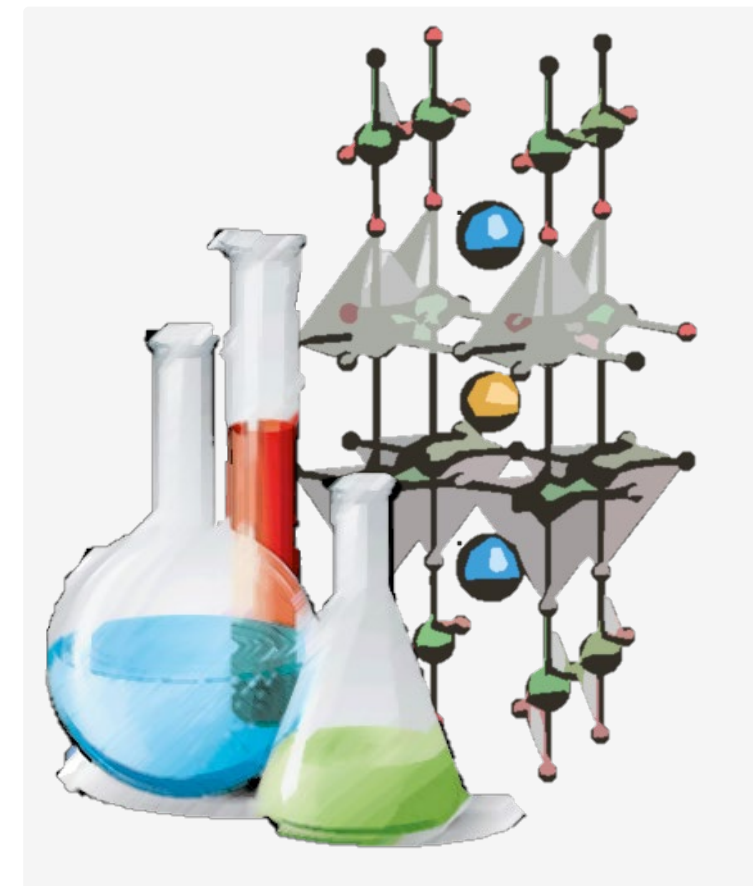


Microstructural landscape and vortex pinning scenarios in REBCO coated conductors prepared at high growth rates

Xavier Obradors

Teresa Puig, Joffre Gutiérrez

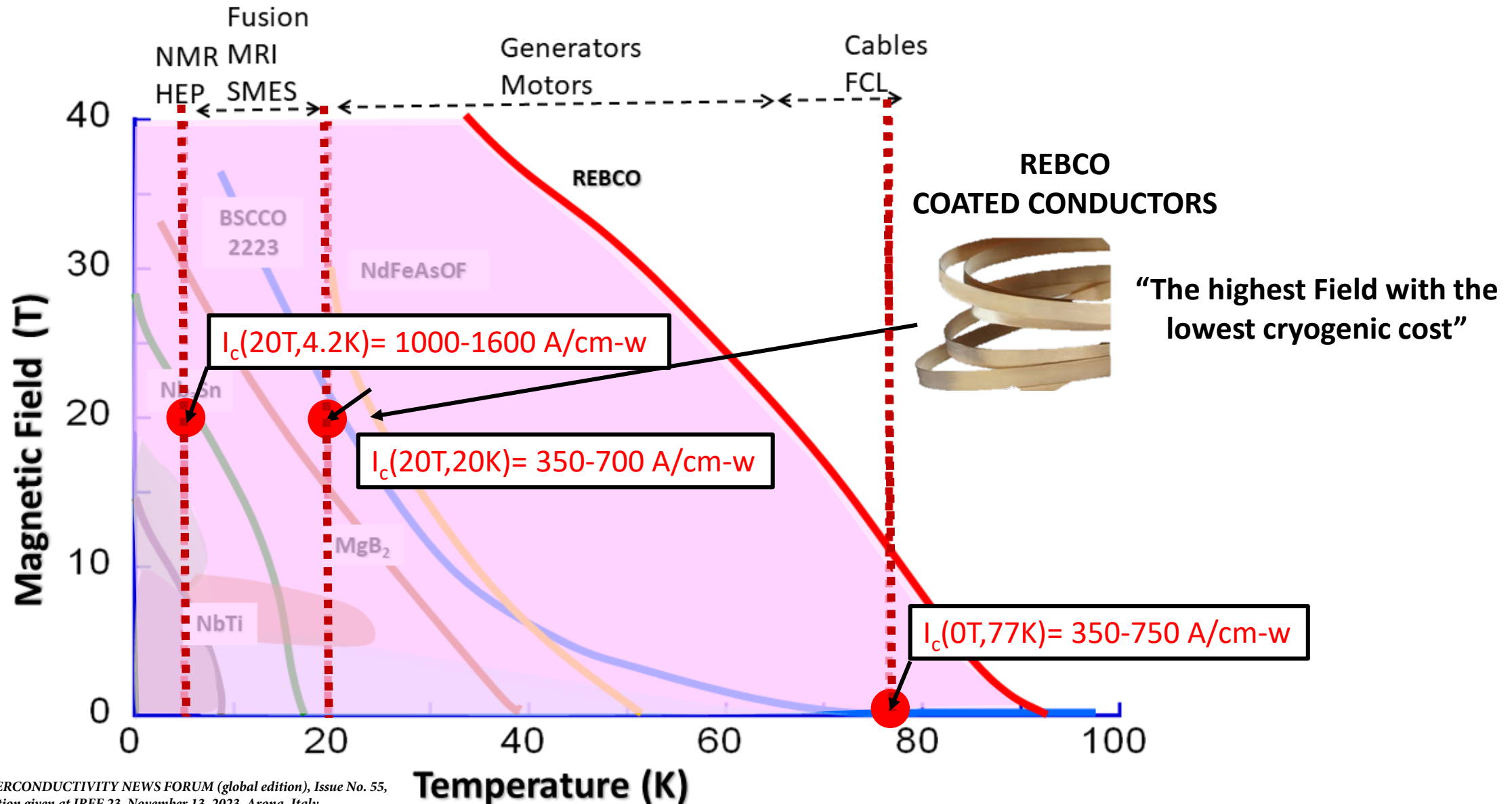
*Institut de Ciència de Materials de
Barcelona, ICMAB-CSIC, Catalonia, Spain*



Motivation and outline

- Exceptional properties of REBCO Coated conductors at ultrahigh magnetic fields: excellent opportunity for compact fusion
- UHF magnets (20 T / 20 K) for fusion require extremely long lengths of CCs (~ 20.000 km/magnet) with high performance (I_c (20T, 20 K))
- High throughput production of CCs is essential to cope with the expected demands: High growth rates of CCs need to be developed
- Understanding the impact of high growth rates on the microstructure and vortex pinning mechanisms of CCs is essential to optimize the potential of CCs
- Reliable methodologies to analyse the influence of high energy neutron irradiation in CCs are required
- Overview of vortex pinning scenarios of CCs prepared at high growth rates

REBCO coated conductors: enabling a new era of fusion energy



The prospects of high-temperature superconductors

Overcoming cost barriers could make high-temperature superconductors pervasive

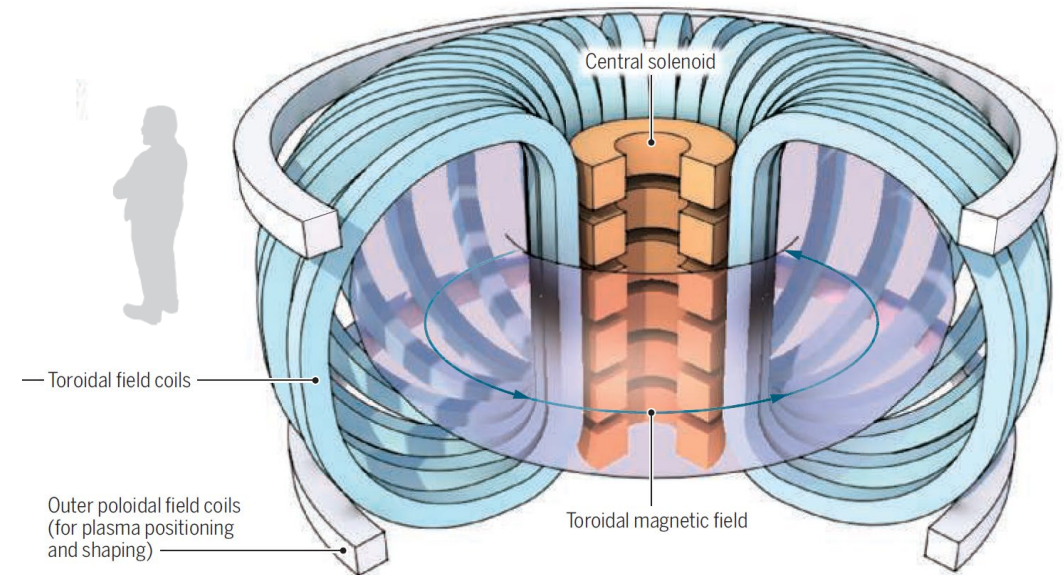
By Alexander Molodyk¹ and David C. Larbalestier²

Science **380**, 1220, 2023

“...the present outlook for high-temperature superconductor materials and their industrial applications is historic...”

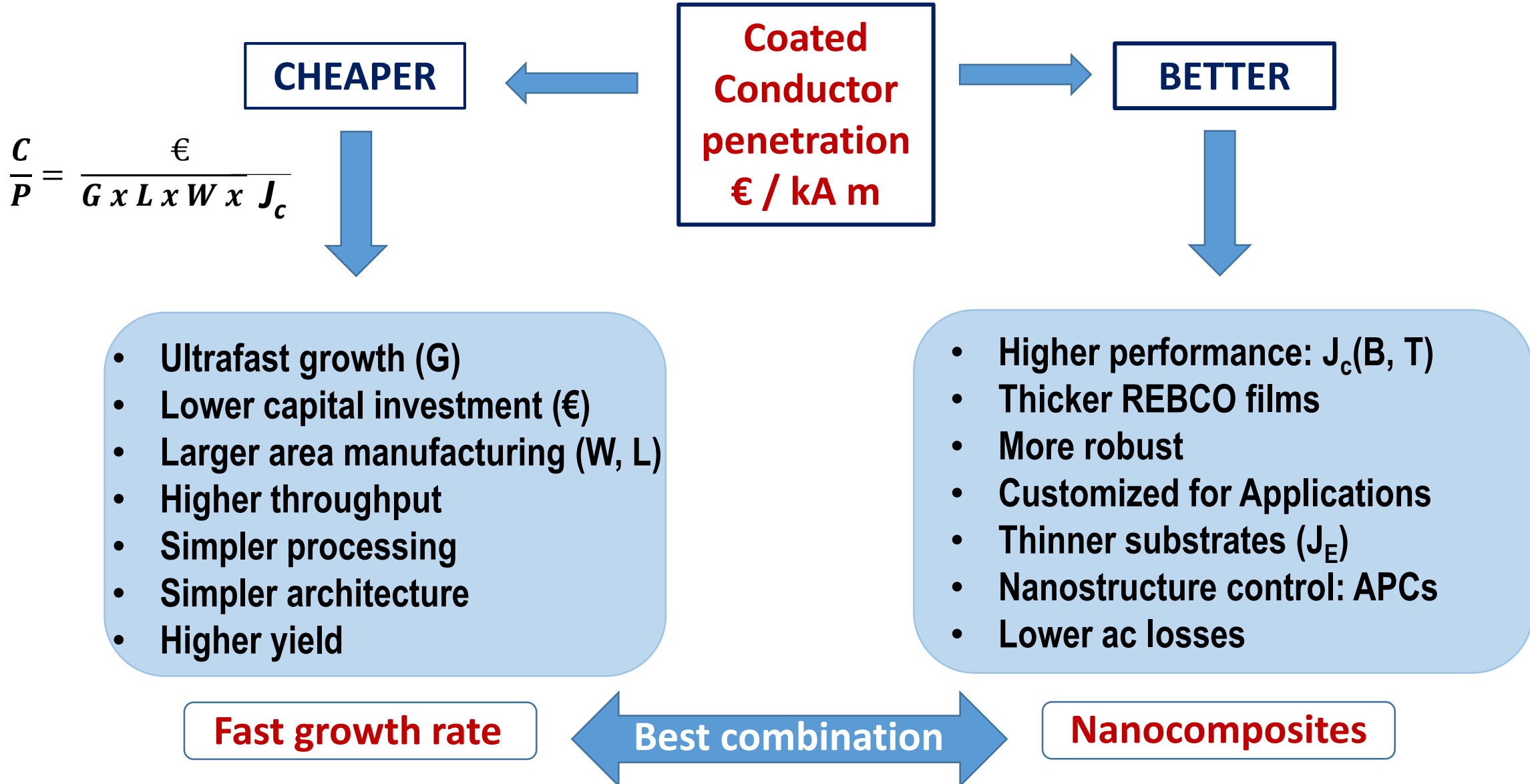
The applied superconductivity community is anticipating the virtuous cycle of price reduction and further demand from other electrotechnology applications that are not yet economic at today's REBCO CC prices

COMPACT FUSION

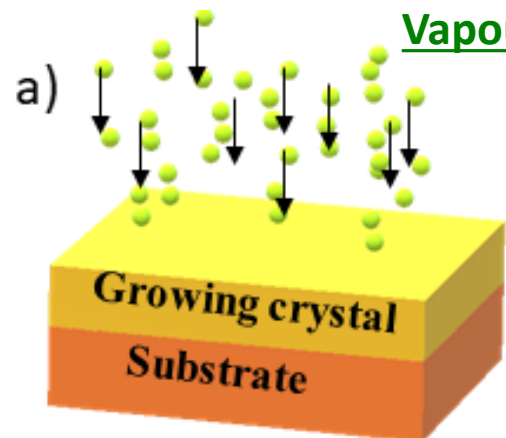


The development of compact nuclear fusion power generation is the immediate stimulus that has driven exponential annual volume increases.

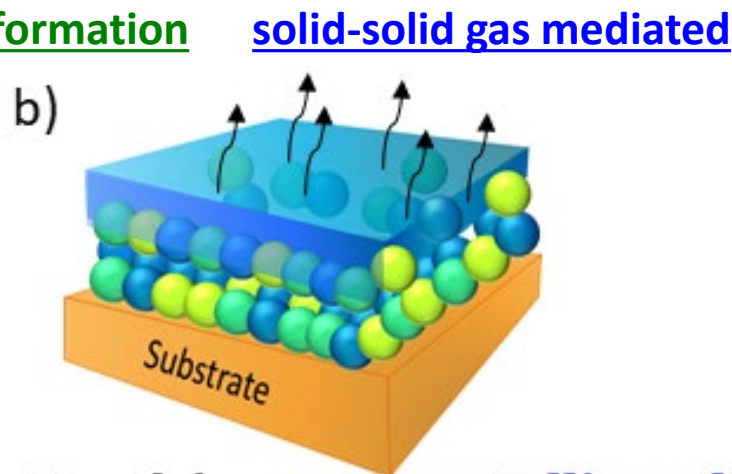
Coated Conductors: materials objectives



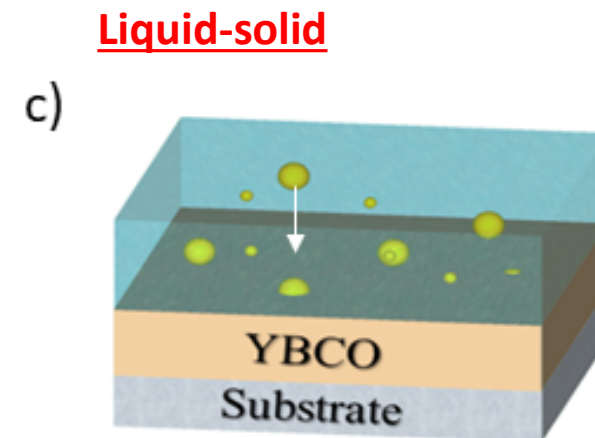
REBCO growth processing: simultaneous and sequential



Growth from **vapour phase**
PLD, MOCVD, ME, MBE, Sputt



Growth from **nanocrystalline solids**
TFA₇-MOD, BaF₂



Growth from **liquid phase**
TLAG-CSD, RCE-DR, HLPE, VLS

Supersaturation, σ , is the driving force for crystallization: $\sigma \propto G$ (growth rate)

$$\sigma = (P_{ad} - P_{ad,e}) / P_{ad,e}$$

Deposition rate
High vacuum environ.
Simultaneous

$P_{ad,e}$ = ad-atoms equilibrium pressure at surface growth front

P_{ad} = ad-atoms pressure at surface growth front

Growth rate: **G = 0.5-25 nm/s**

$$\sigma = f(\ln(P_{HF}^2 / P_{H2O}))$$

P_{HF} = HF partial pressure

P_{H2O} = water partial pressure

Sequential

G = 0.5-5 nm/s

$$\sigma = (C_{\delta} - C_e) / C_e$$

RE solubility,
Ba-Cu-O liquid

C_e = RE equilibrium concentration in the liquid

C_{δ} = RE actual concentration

Simultaneous or sequential

G = 10-1000 nm/s

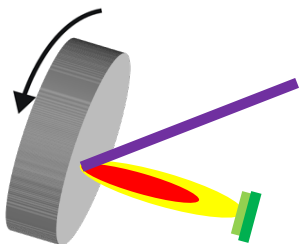
Transient Liquid Assisted Growth (TLAG)

A new high throughput non-equilibrium kinetically controlled growth process



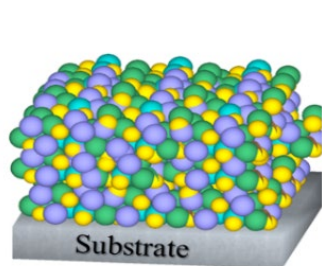
CSD

L. Saltarelli et al, ACS Appl. Mat. & Interf. (2022)

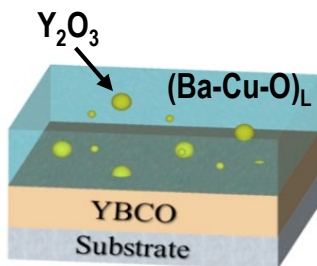


Low Temp PLD

A. Quetalto et al, SUST (2023)



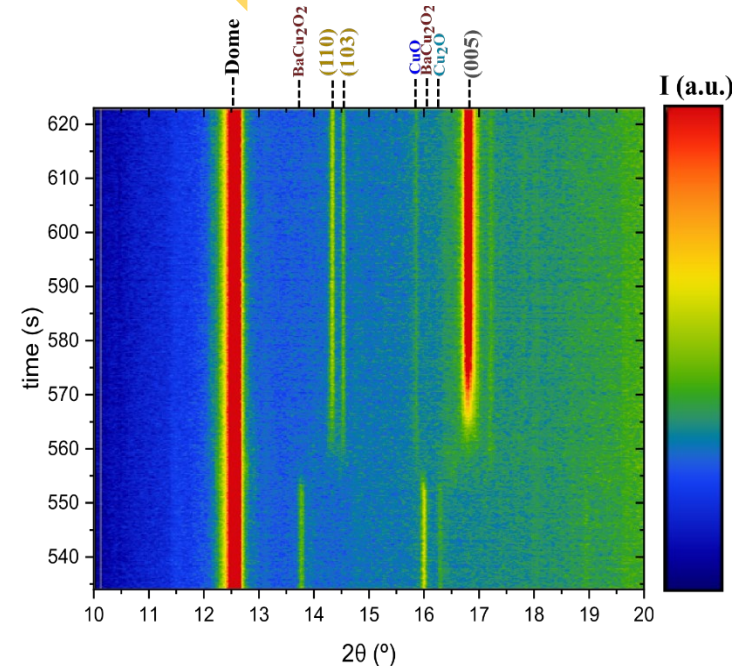
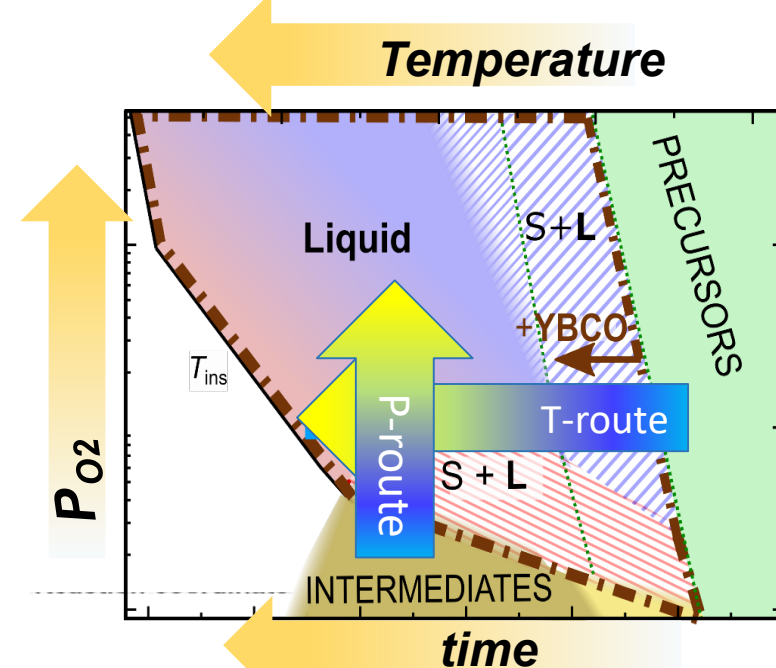
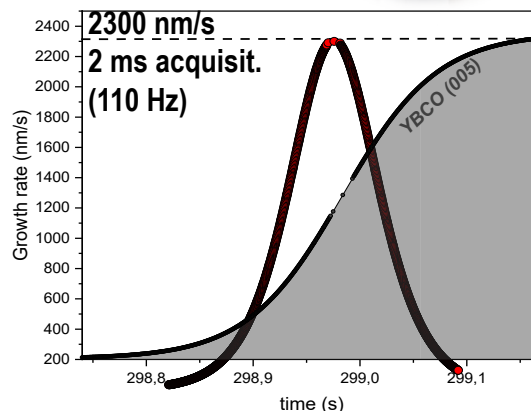
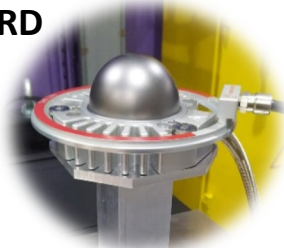
Nanocrystalline precursors



YBCO growth

- High performance (3 MA/cm² at 77K)
- High throughput
- Simple reactor
- Large area processing
- Low cost/performance method

In-situ synchrotron XRD



100 nm/s by **ultrafast-PLD** EuBCO/BHO
(transient liquid growth at high T PLD)

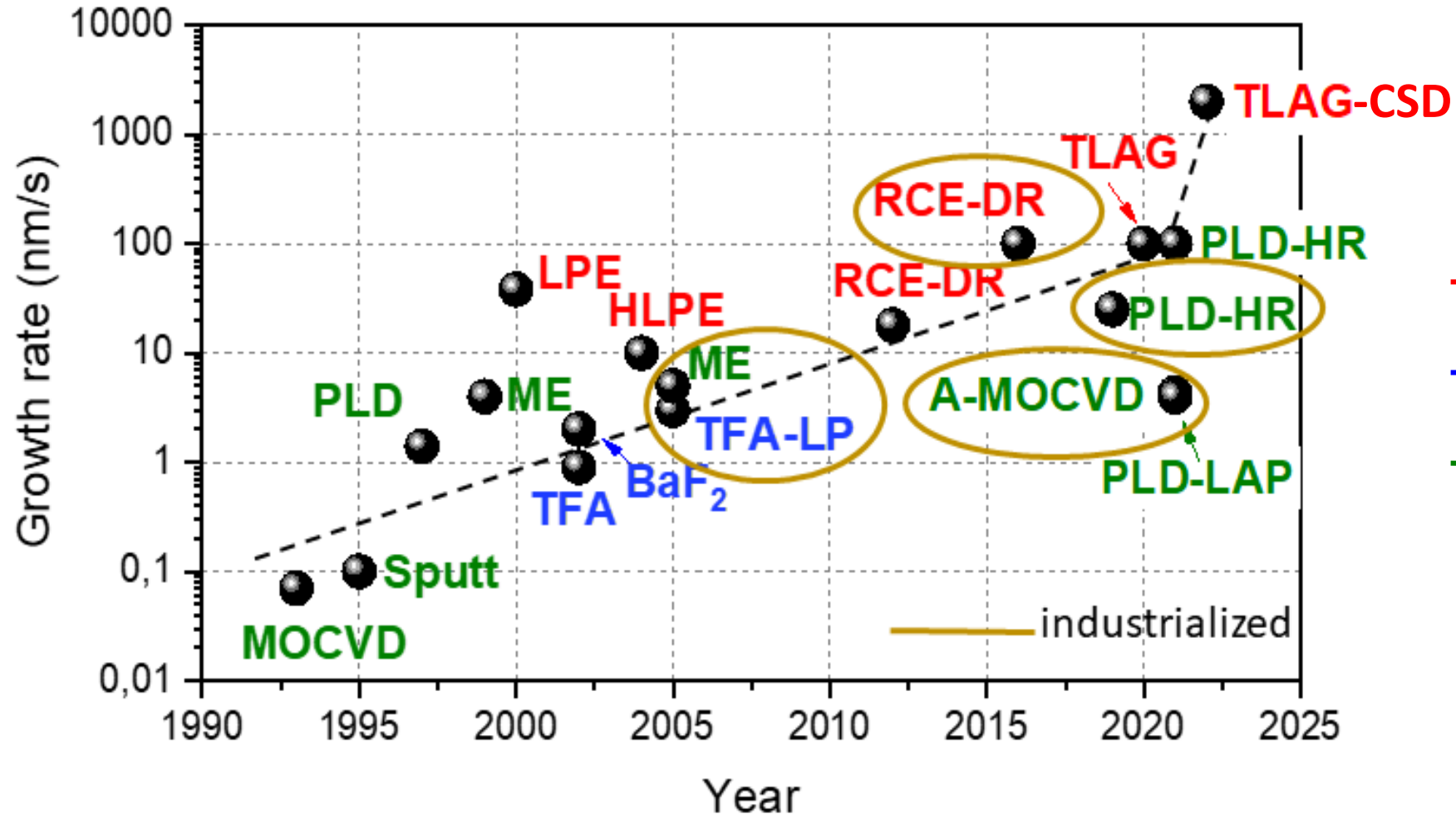
Y. Wu, Materials & Design 224 (2022)

L. Soler et al., Nat Comm (2020), S. Rasi, et al, Advance Science (2022)

Reaching high Growth Rate: A path towards cost reduction

Figure of merit: $\frac{Cost}{Performance} = \frac{total\ cost\ per\ year}{G \times L \times W \times (I_{c-w}/d)} = \frac{\text{€}}{kA \times m}$

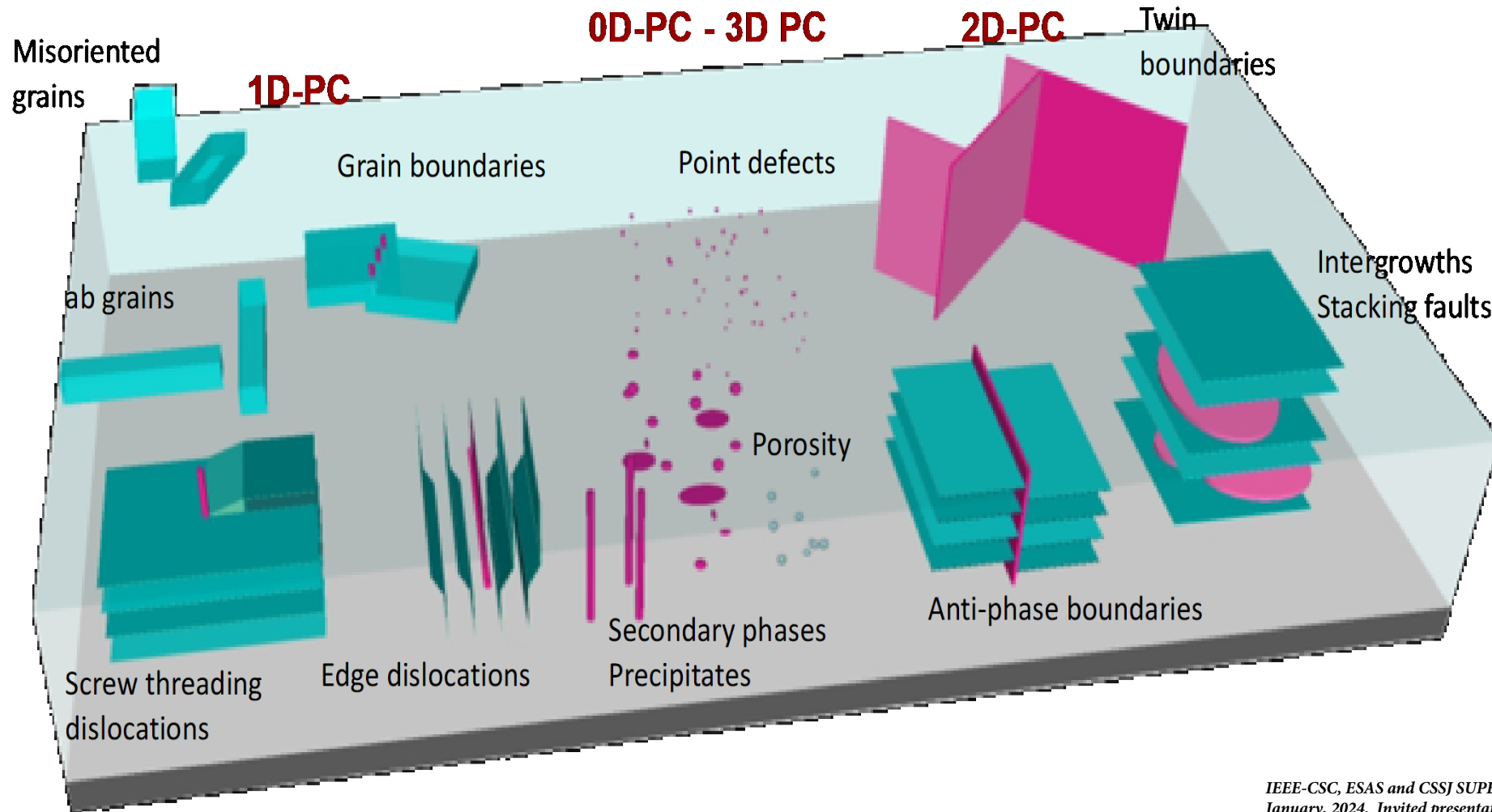
W = tape width
 L = tape length
 d = tape thickness



The complex defect structure in nanocomposites

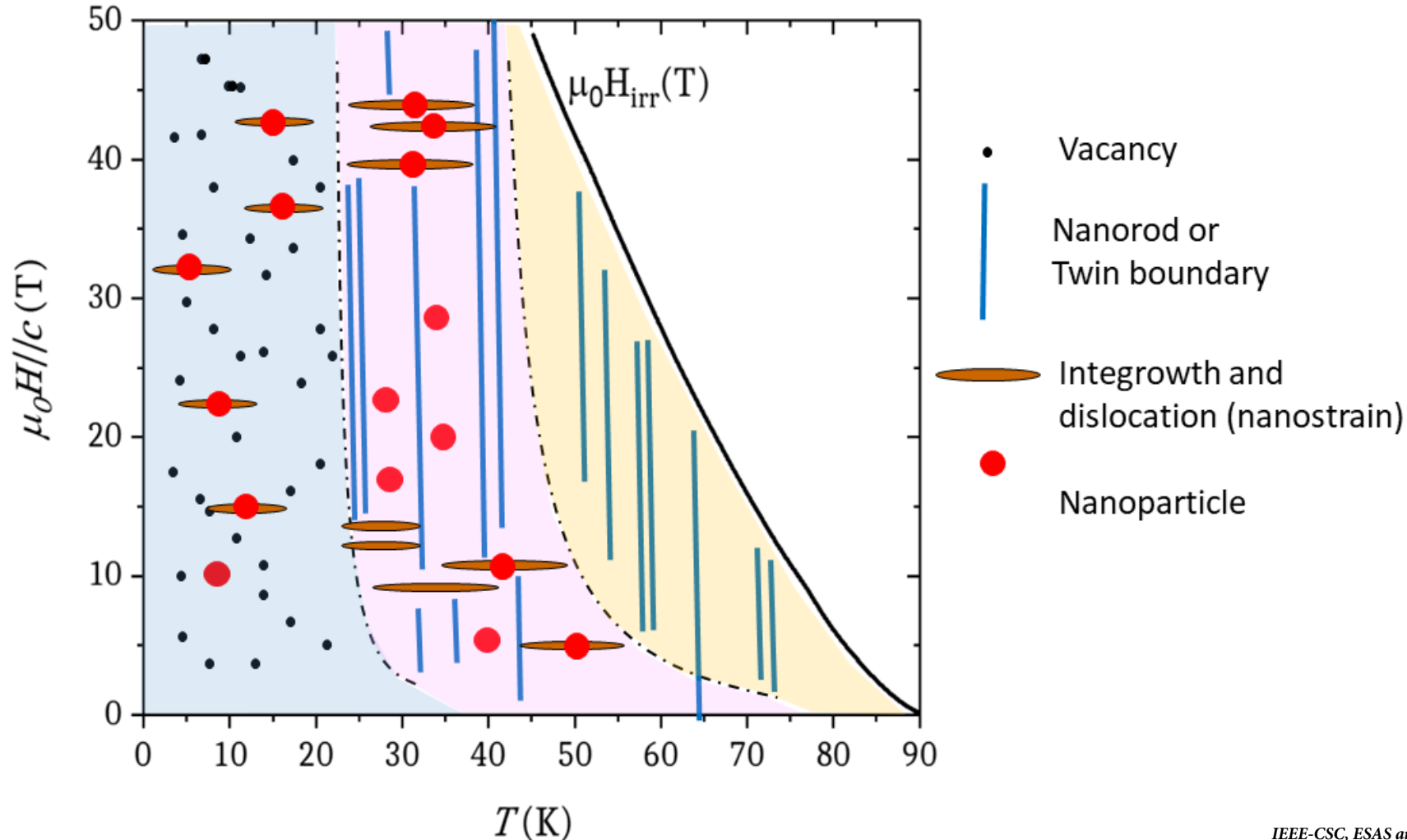
Relevant issues: size, dimensionality, orientation, concentration

Different growth methods have modified nanostructures



The complex magnetic phase diagram of nanocomposites

Relevant issue: behaviour of defects as APCs can be classified as weak or strong and isotropic or anisotropic



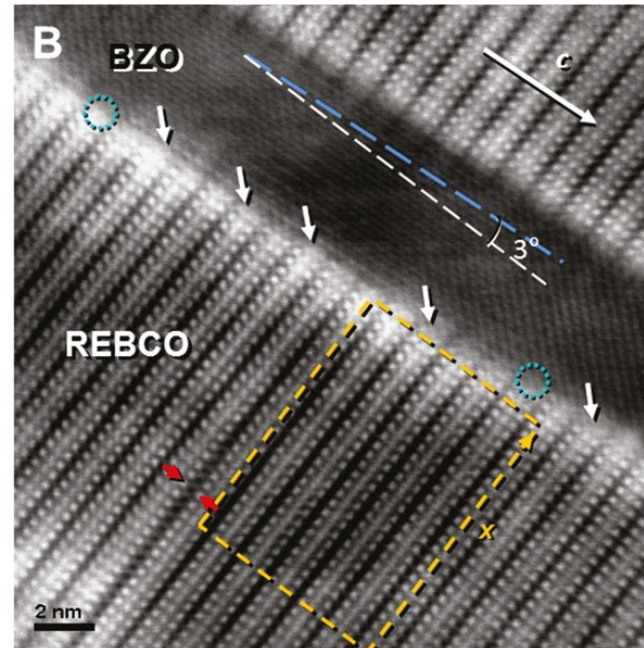
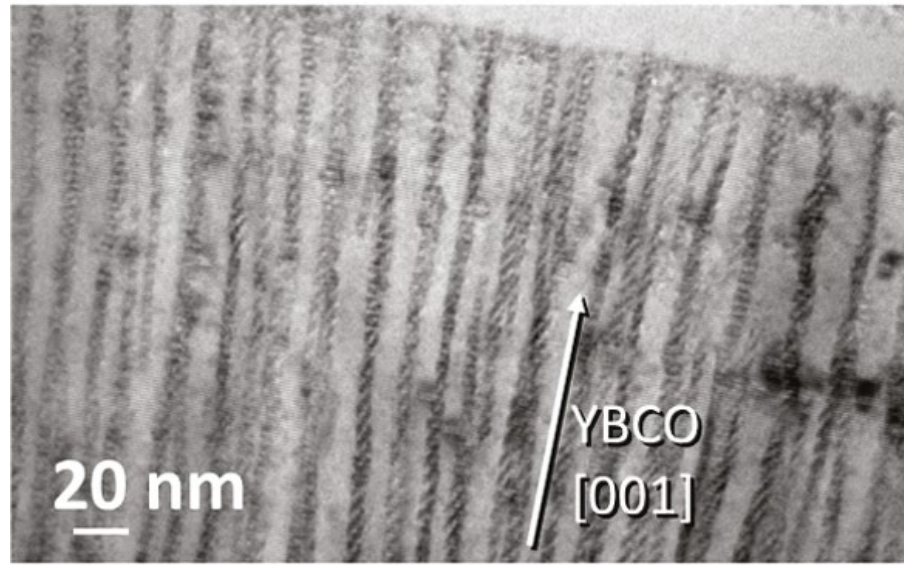
We need a simple route to classify defects behaviour in terms of vortex pinning centers to follow the differences and the evolution of CCs with different processing methodologies and now with irradiation !

Simultaneous deposition/growth: micro/nanostructure

BaZrO₃ nanocolumns

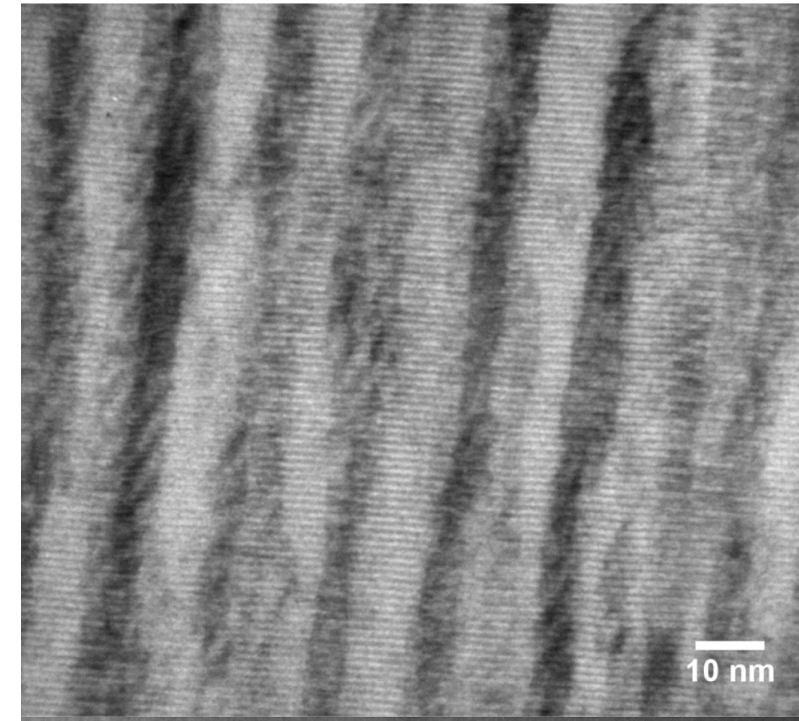
PLD

Vapour - solid growth: **low growth rates** (1 - 4 nm/s)



(Gd,Y)BCO / BZO nanorods
5-6 nm diameter, separation : 18 nm
Growth rate: 4 nm/s

A-MOCVD



Strain field develop around the nanocolumns to reduce boundary energy inducing self-assembly
Oxygen vacancies and misfit dislocations at the interface

C. Cantoni et al , ACSNano (2011)

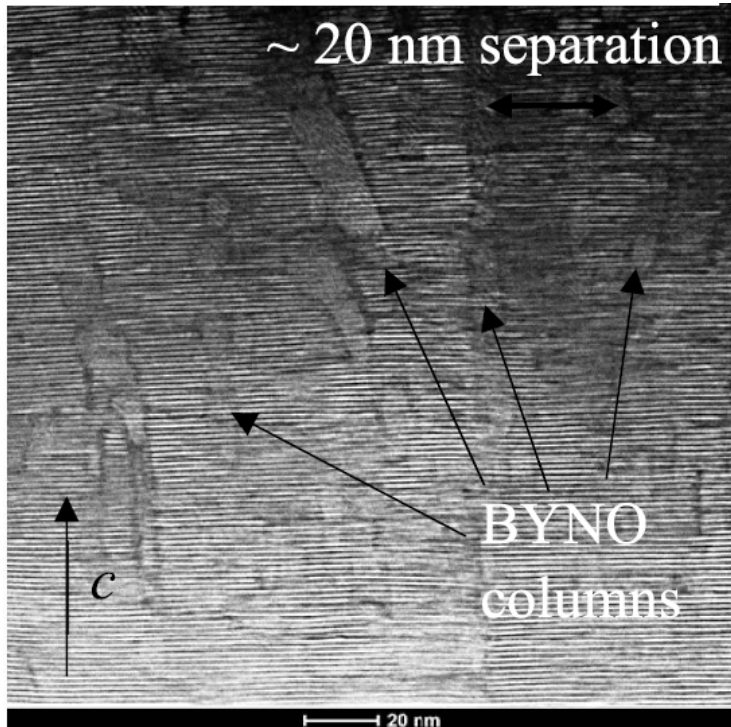
Nanorods (BZO) + nanoparticles (Y₂O₃): Maiorov et al. Nature Mat. 8 (2009)

Nanoparticles (Y₂O₃): Molodyk et al. Sci Reports (2021)

G. Majkic et al., SUST (2020)

Simultaneous growth films: micro/nanostructure

PLD-LAP (YBCO-BYTO)

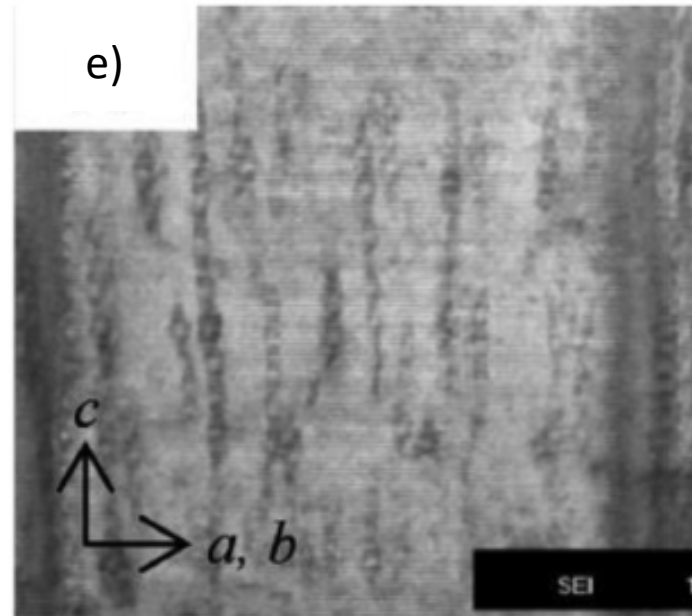


4 nm/s: BYTO nanorods
misalignment

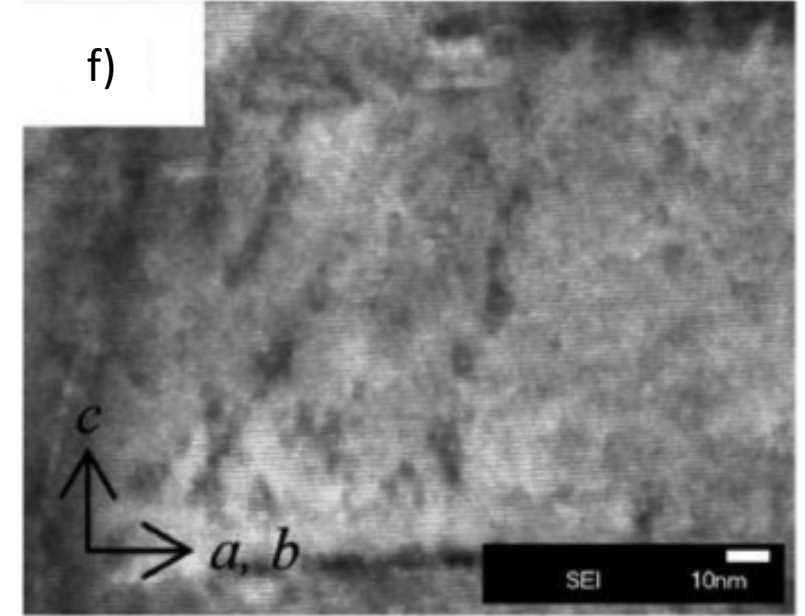
J. Feighan et al., SUST (2021)

Liquid assisted growth: **fast growth rates** (5 - 100 nm/s)

PLD-HR (EuBCO- BHO)



5 – 15 nm/s: discontinuous
aligned BHO nanorods

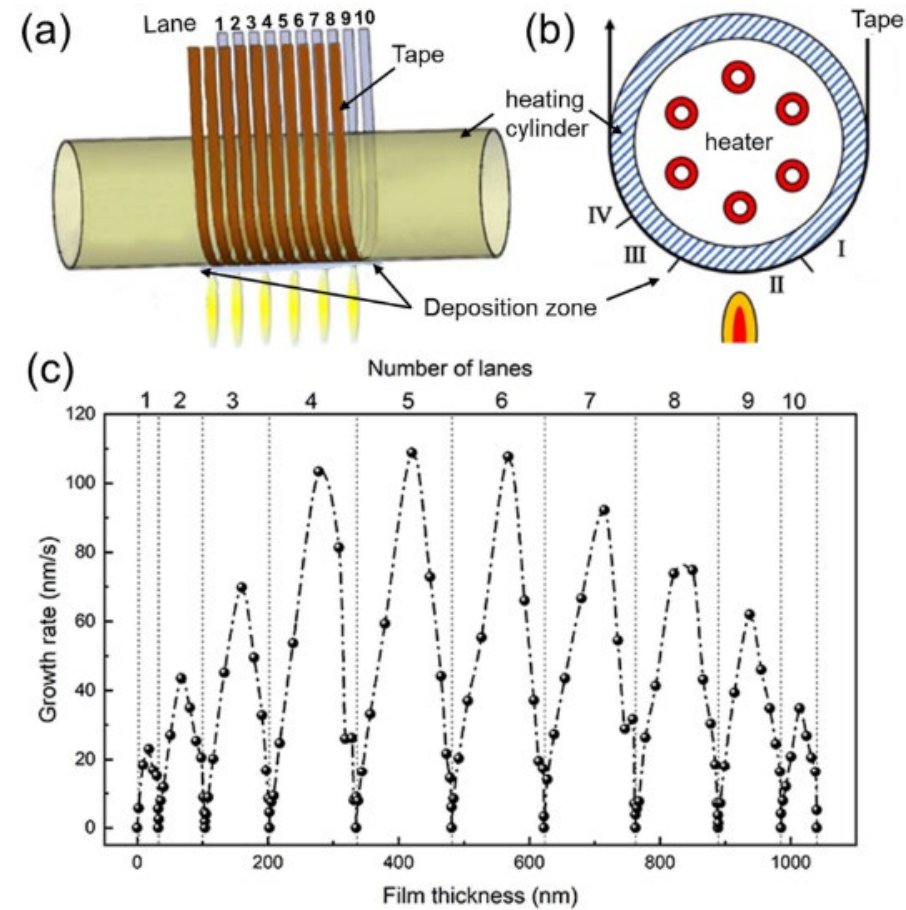


20 – 30 nm/s: strongly
segmented and misaligned BHO
nanorods

S. Fujita et al., IEEE Trans Appl Supercond. (2019)

Simultaneous growth films: micro/nanostructure

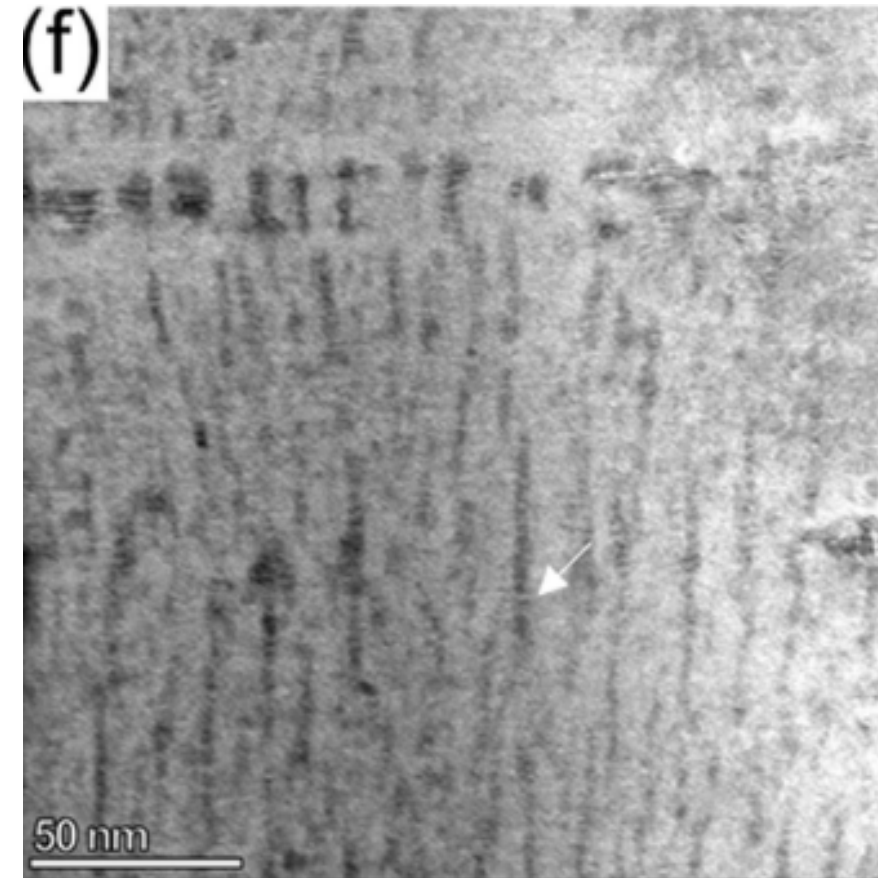
Liquid assisted growth: **fast growth rates** (20 - 100 nm/s)



4 nm/s: BYTO nanorods
misalignment

Y. Wu et al., Mat & Design (2022)
Shanghai Superconductor Technology

PLD-HR (*EuBCO- BHO*)

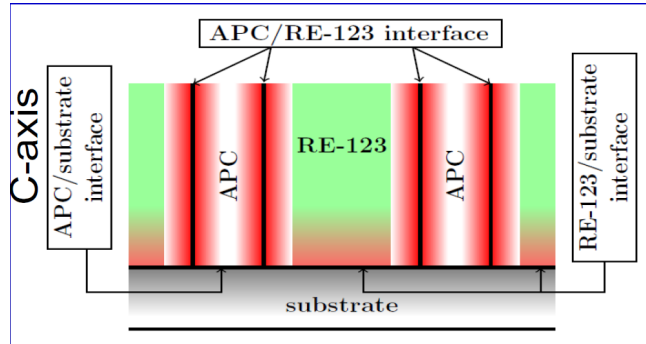


20 – 100 nm/s: strongly segmented
and misaligned BHO nanorods

Simultaneous growth of Nanocomposites

Low versus high growth rate

Grown at 0.6 nm/s

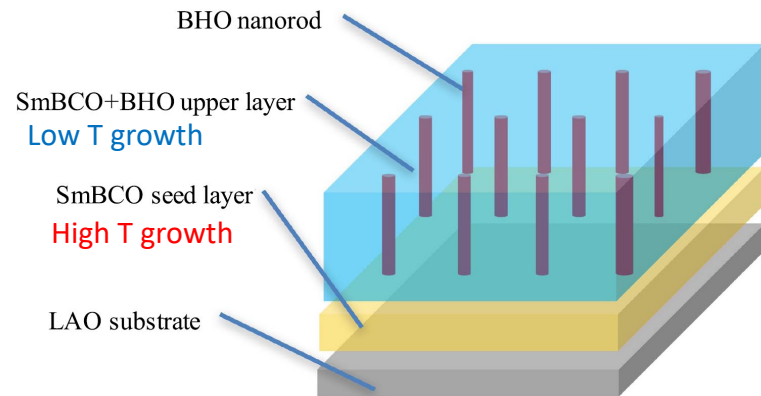


Elastic Strain energy model

Wu, et al, SUST 30 (2017)

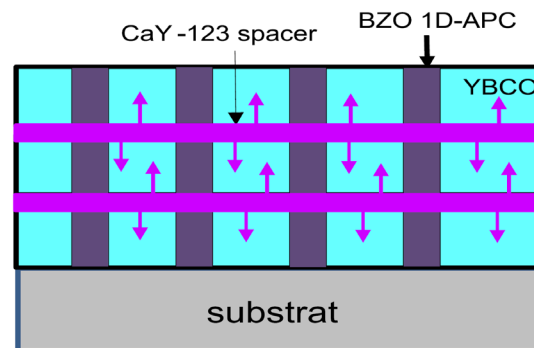
Engineering landscape by design

LTG – PLD method



Y. Yoshida et al, SUST 30 (2017)

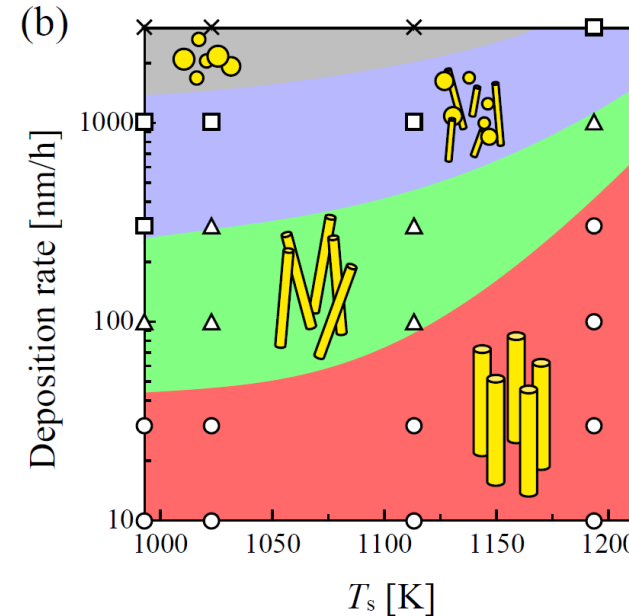
dynamic control of nanorod / YBCO interface



Wu, et al, SUST 35 (2022)

High growth rates (10-50 nm/s)

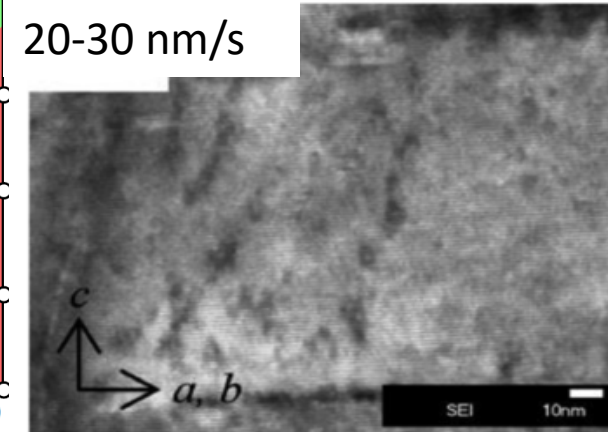
Montecarlo simulations



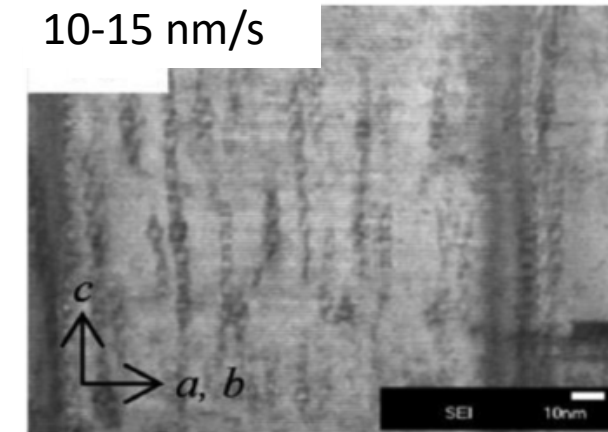
Y Ichino et al J.JAP 56 (2017)

EuBCO + HfBaO₃ nanorods

20-30 nm/s



10-15 nm/s

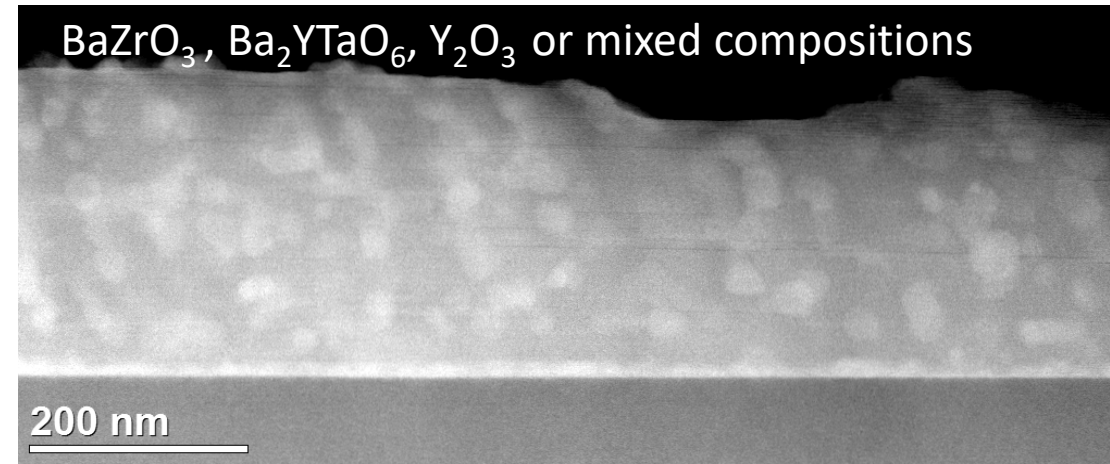
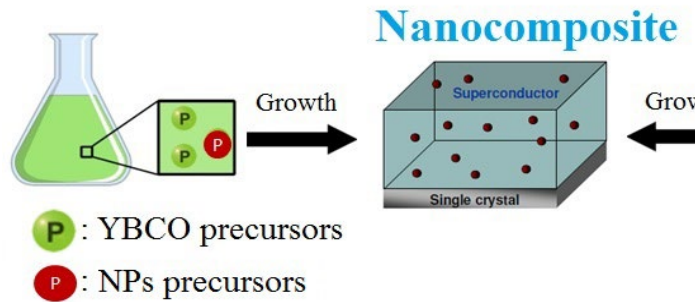


Fujita, S. et al. IEEE TAS 29 (2019)

Sequential deposition and growth films (CSD, RCE-DR)

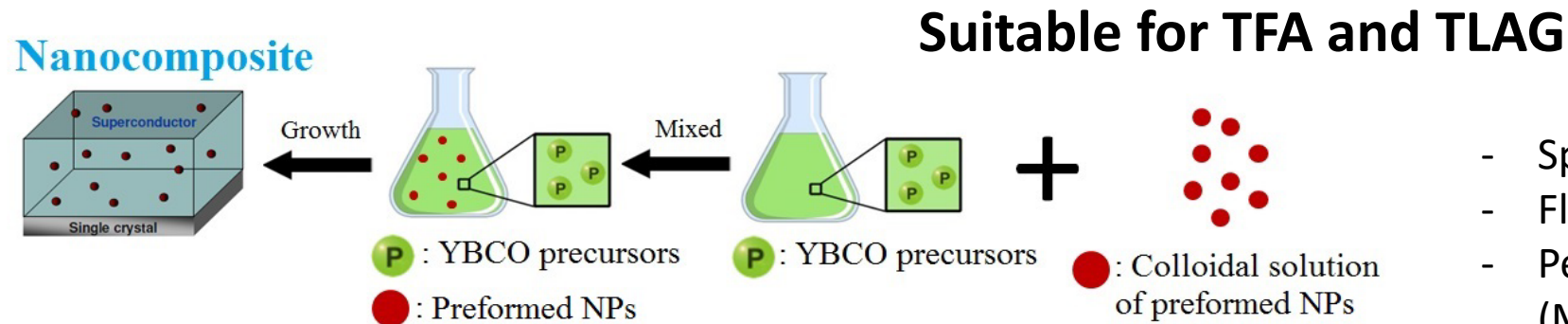
Use of complex solutions for **spontaneous segregation** of nanoparticles (TFA)
(BaZrO_3 , BaHfO_3 , Ba_2YTaO_6 , BaCeO_3)

- J. Gutierrez et al, Nat Mat (2007);
- A. Llordés et al, Nat Mat (2012)



Not suitable for TLAG

pn-Nanocomposites: Colloidal solutions with **preformed nanoparticles** (N. Chamorro, RSC Adv. (2020))



- Spinel (MFe_2O_4)
- Fluorite (CeO_2 , ZrO_2)
- Perovskite BaMO_3 (M= Zr, Hf)
- Bronze $\text{Ba}(\text{Ta},\text{Nb})_2\text{O}_6$

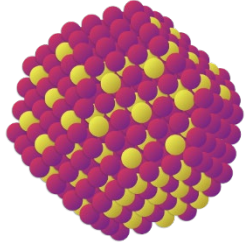
Need to stabilize np in the alcoholic and ionic environment of YBCO precursor solution at high concentrations

- P. Cayado et al, SUST (2015)
- X. Obradors et al, SUST (2018)
- D. Garcia et al., to be published

Nanoparticles for multifunctional colloidal solutions

Requeriments

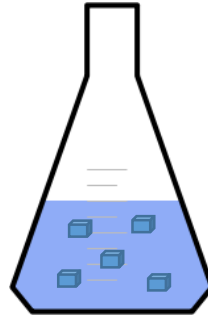
NP solution



Small-size < 10 nm

Non-aggregation
in alcohol solution
High concentrations in
alcohol solution
(≥ 100 mM)

Stabilization in YBCO precursor solution



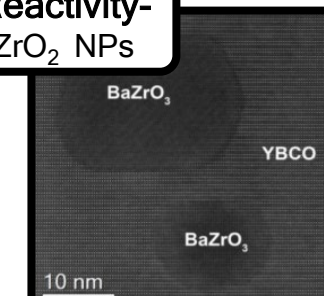
NPs compatible and stable
in YBCO precursor solution
-non- aggregation
-no precipitation

Compatibility with CSD-TLAG process

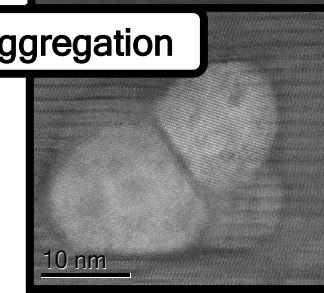
NP composition non-reactive
with YBCO

High-thermal stability of
NP composition

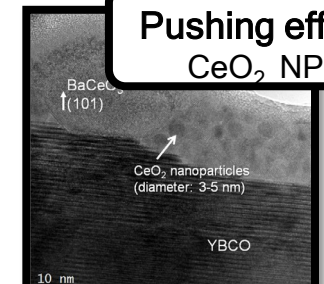
Reactivity-
ZrO₂ NPs



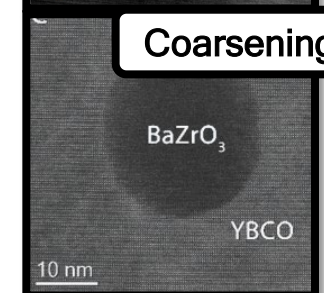
Aggregation



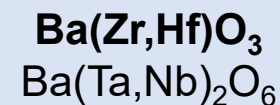
Pushing effect-
CeO₂ NPs



Coarsening

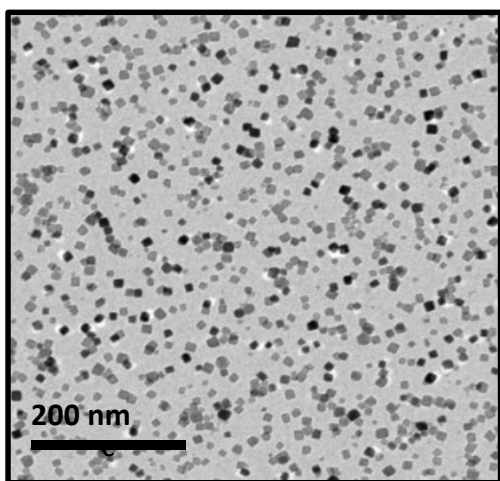
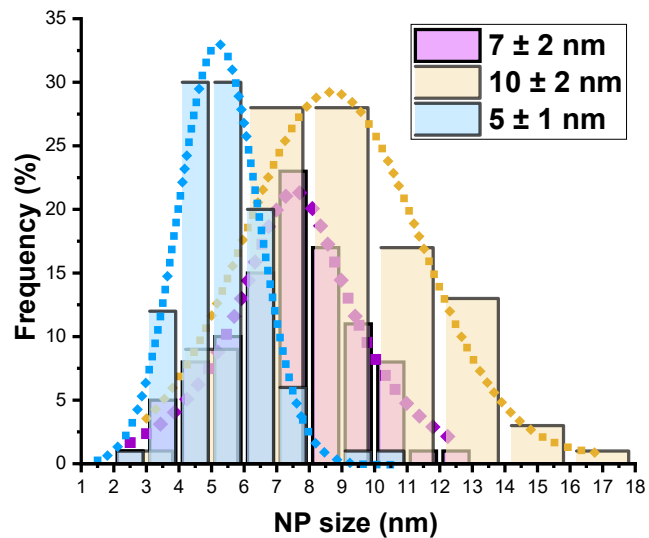


Multifunctional colloidal ink
(Patent EP22382741)



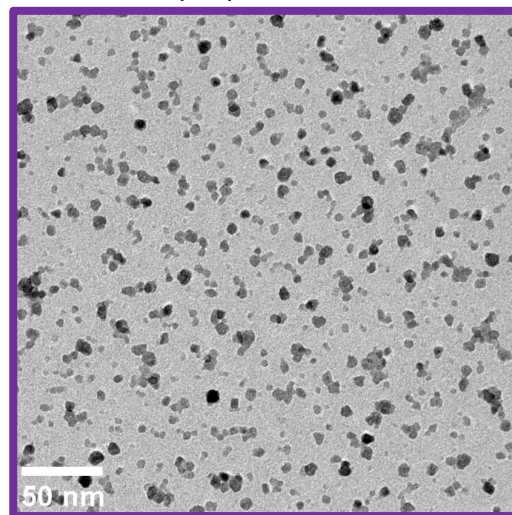
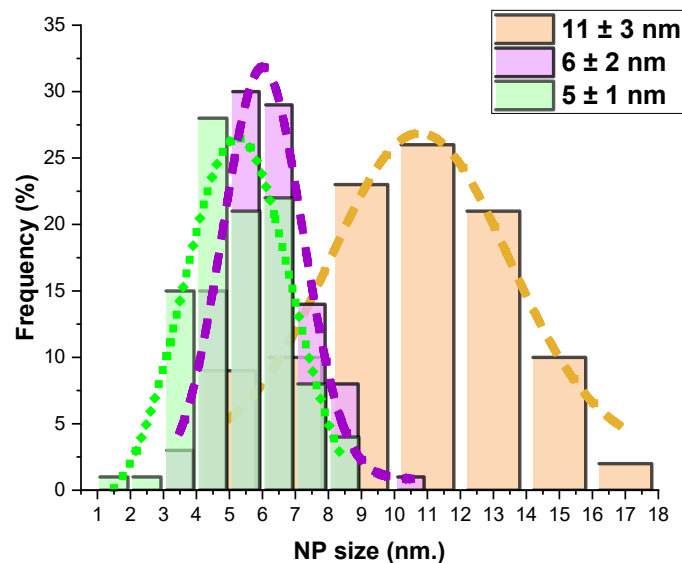
BaMO₃ (M= Zr and Hf) Nanoparticles

BaZrO₃ NC

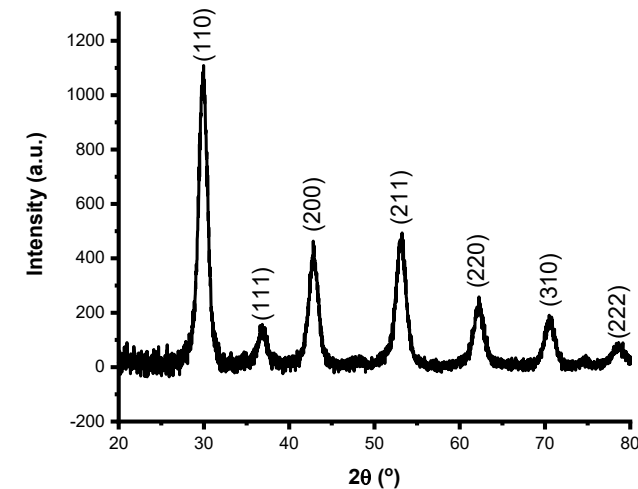
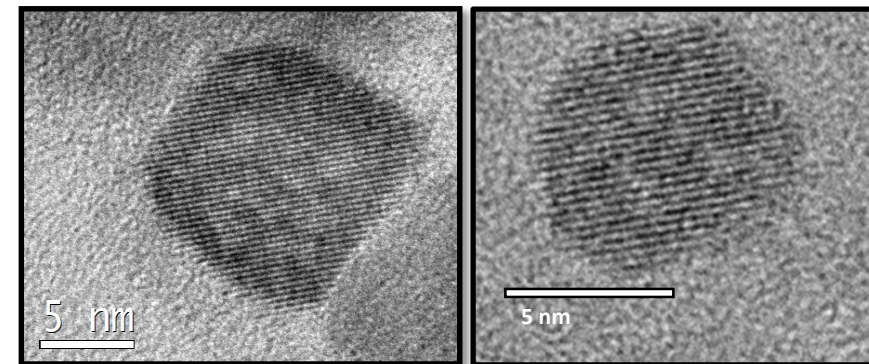


✓ Stable solutions (size/surface stability) for months

BaHfO₃ NC



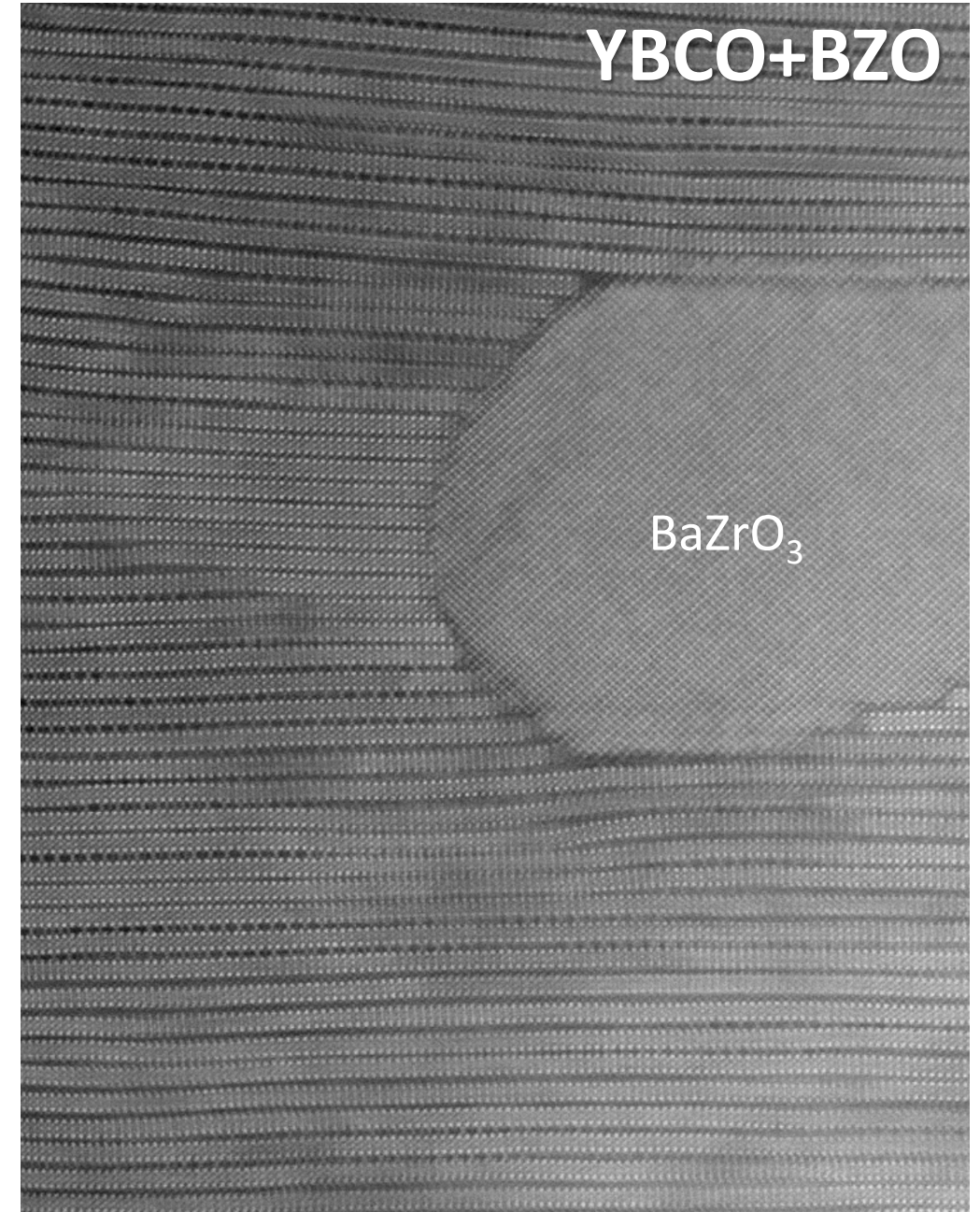
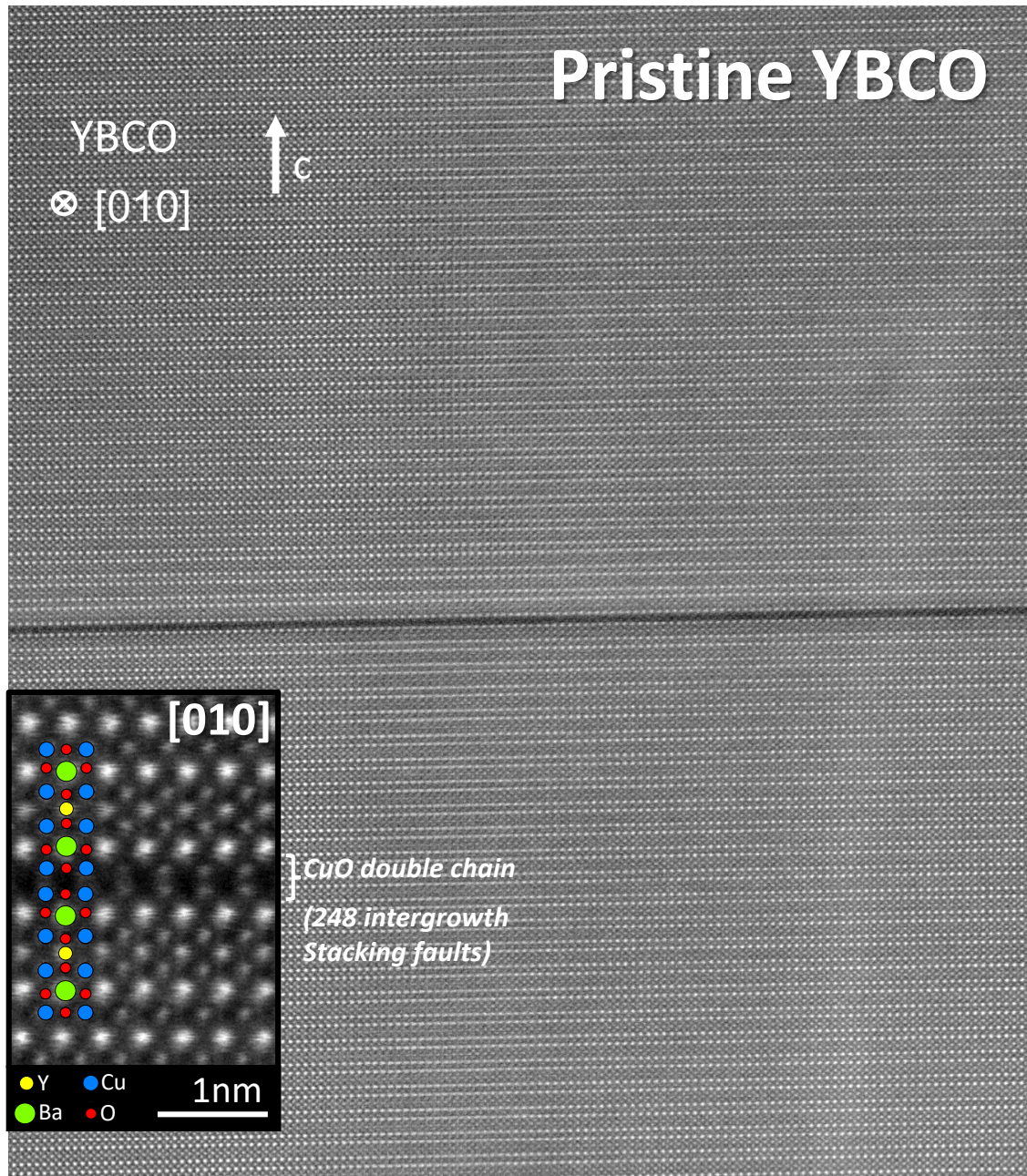
✓ Tuneable NP size from 4-20 nm



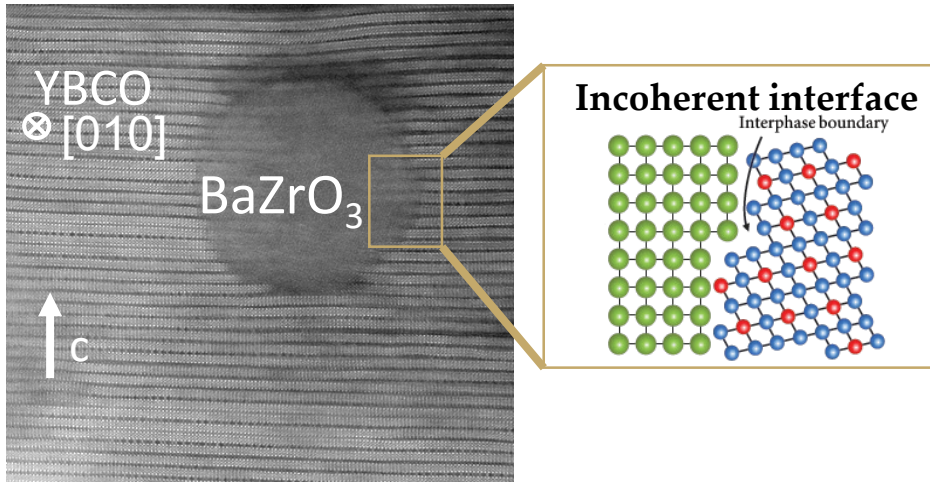
cubic phase

N. Chamorro et al, RSC Adv. (2020)

Nanoparticles induce stacking faults at the incoherent interface

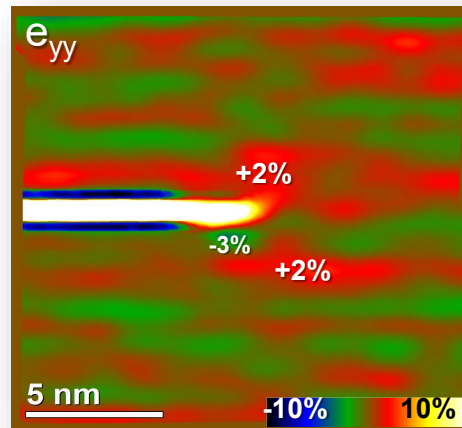


Incoherent YBCO-BaZrO₃ interfaces give rise to high density of Y248 intergrowths and associated nanostrain



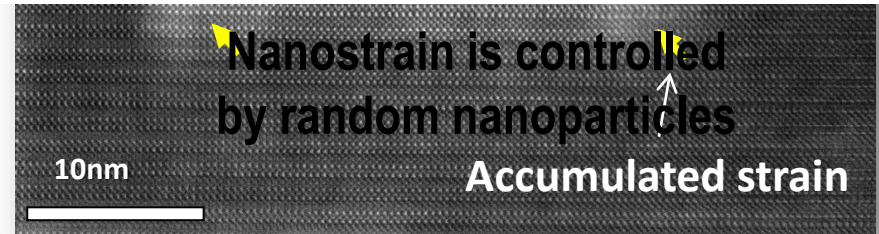
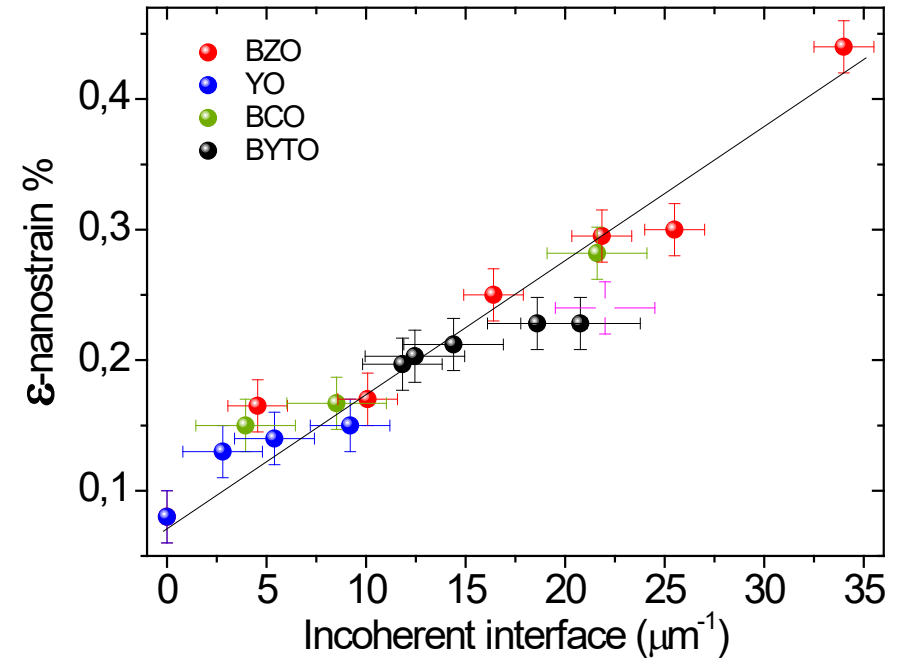
Incoherent interface is associated to the random orientation of the nanoparticles

Strong strain effects are generated at the partial dislocations

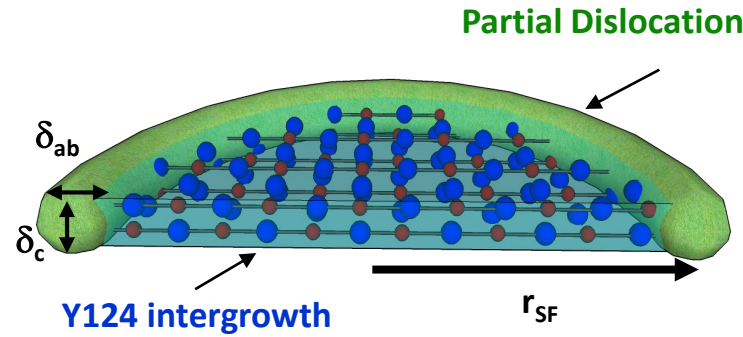
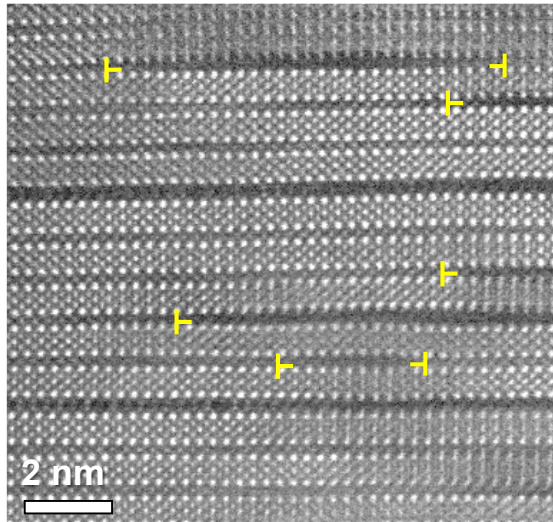


HAADF

TFA Nanocomposites



Partial dislocations surrounding SFs: source of isotropic nanostrain

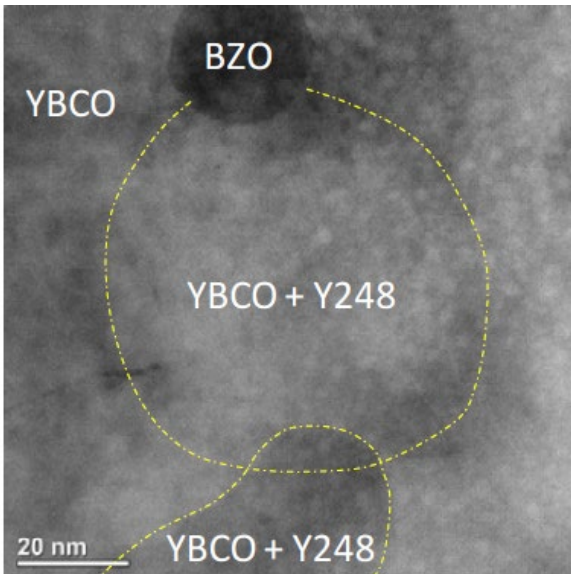


(Dislocation volume density from STEM images)

$$\rho_{dislocation} = \frac{\pi \delta_c \delta_{ab}}{\Delta x \Delta y \langle r_{SF} \rangle} \left(n_{SF} \delta_{ab} + 2 \sum_{i=1}^{n_{SF}} r_{SF_i} \right)$$

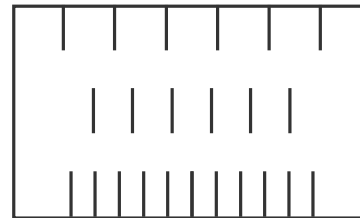
Nanostrain can be easily measured by XRD and it controls the concentration of dislocations (TEM analysis) and nanometric disorder.

Vortex pinning is closely correlated to nanostrain

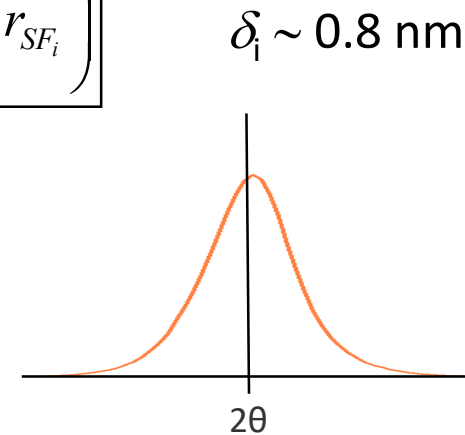


Plan view TEM

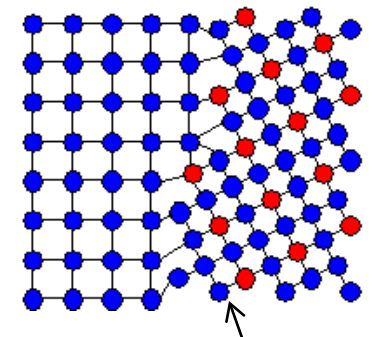
$\epsilon = \Delta d/d$
d-spacing fluctuations
↓
defects



Non-uniform strain (nanostrain)

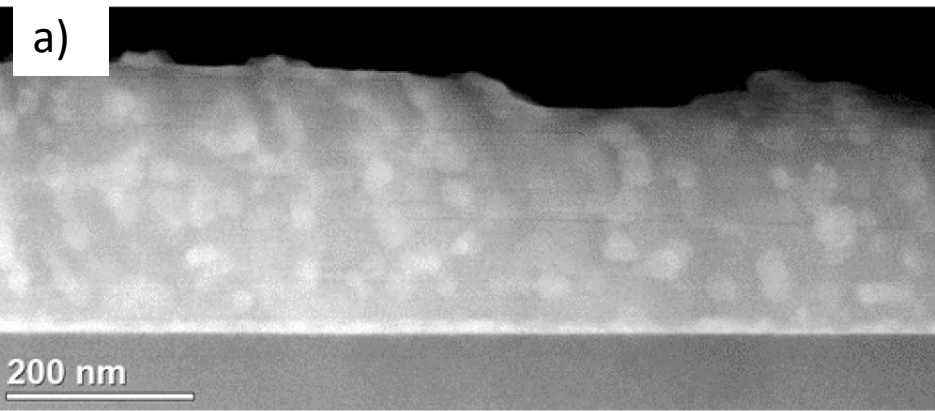


Williamson-Hall plot

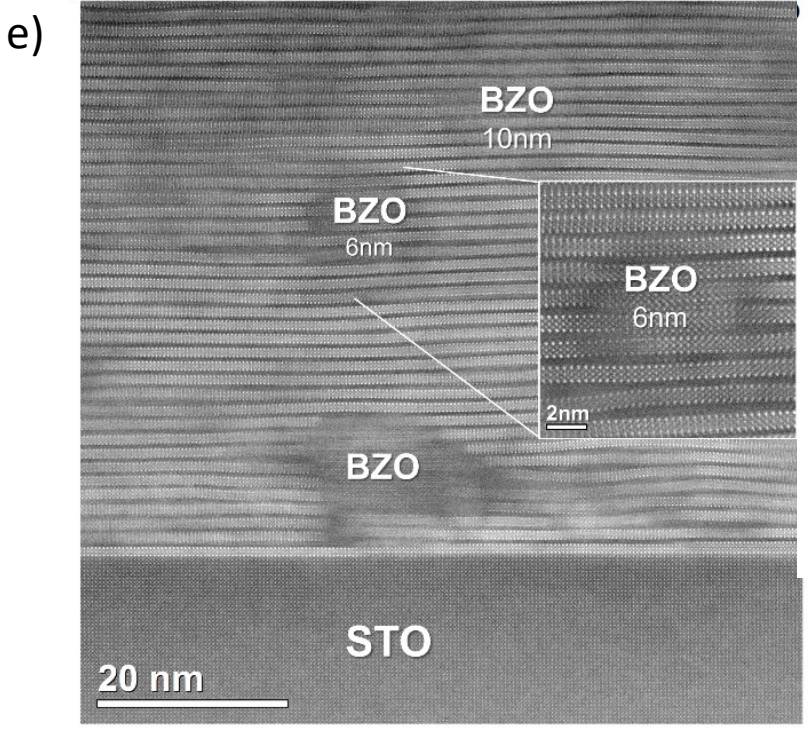
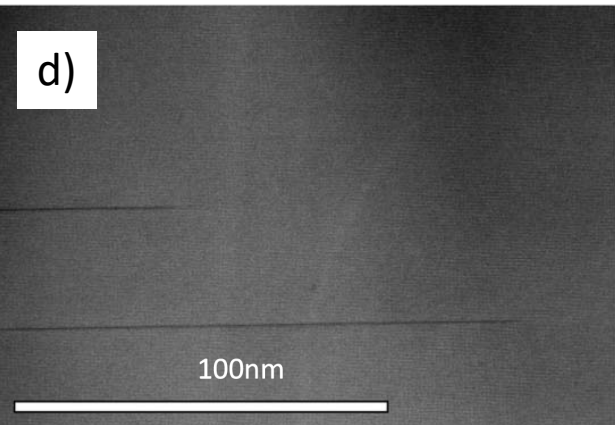
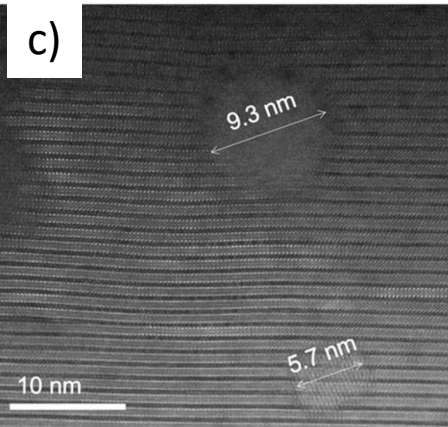
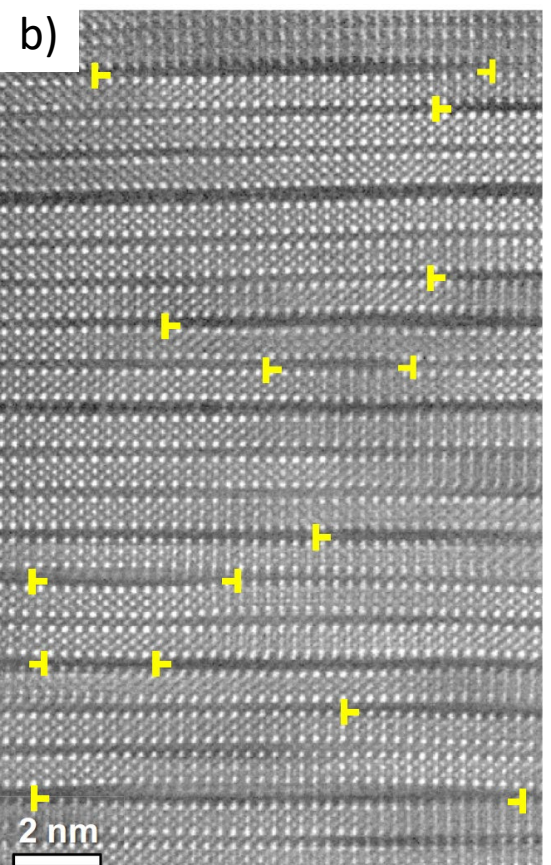


incoherent interface

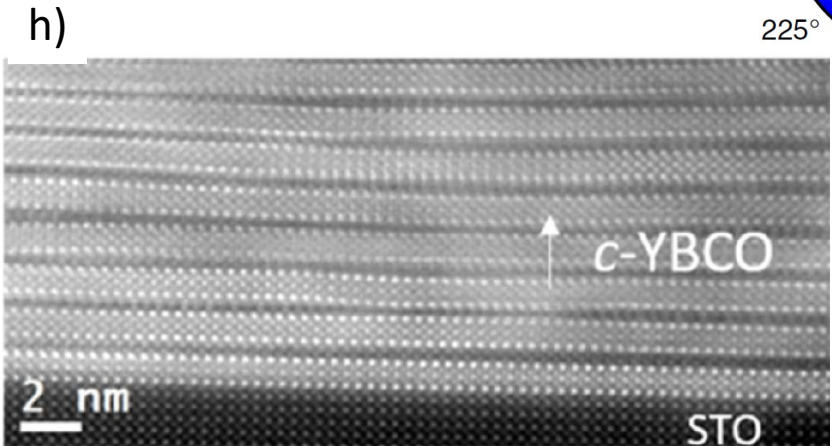
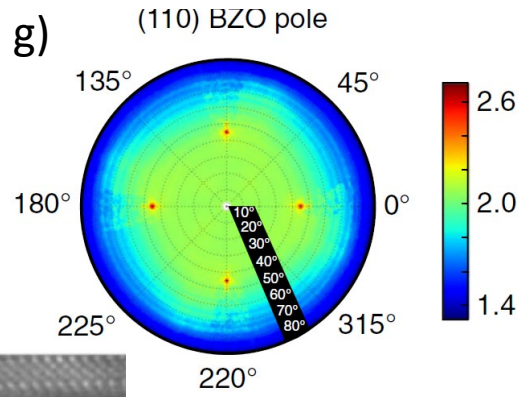
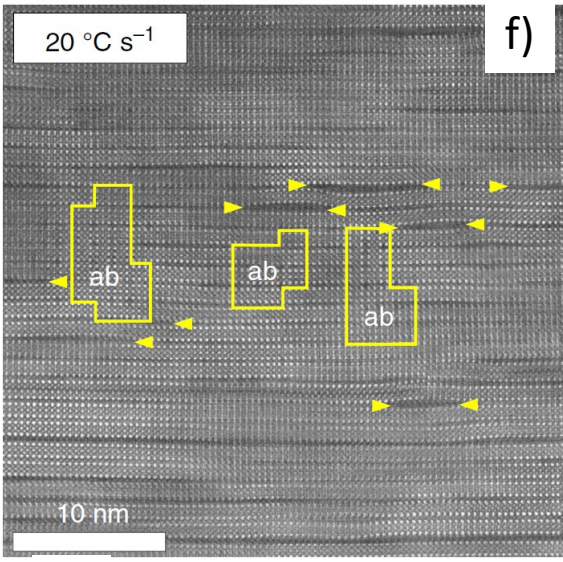
Sequential deposition and growth films: micro/nanostructure



TFA



TLAG

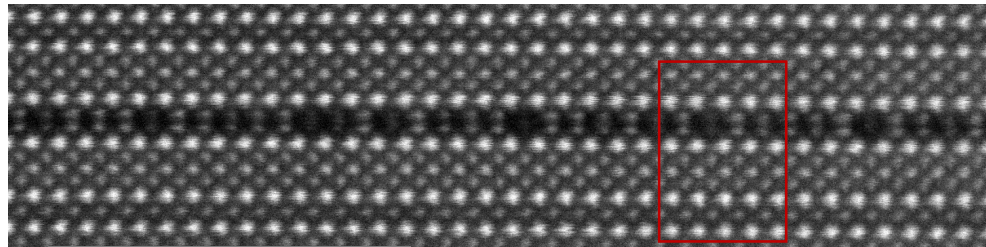


Weak pinning contribution: cation-oxygen vacancy clusters

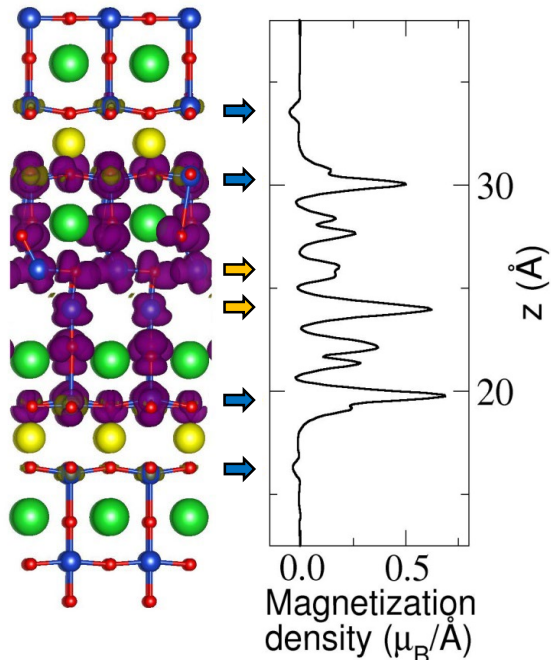
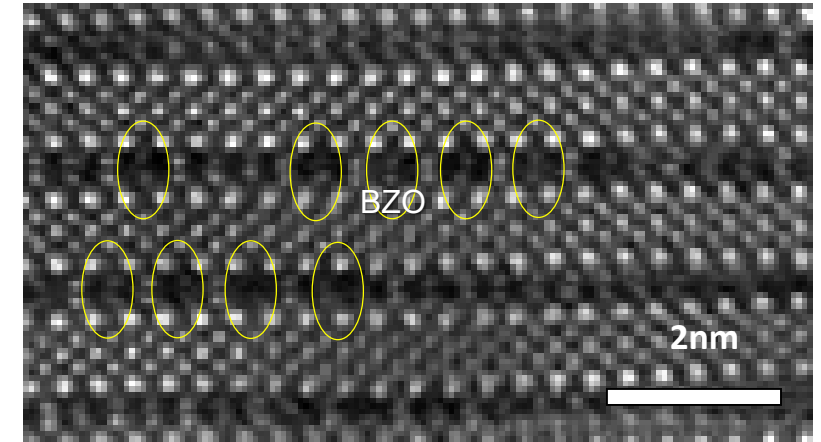
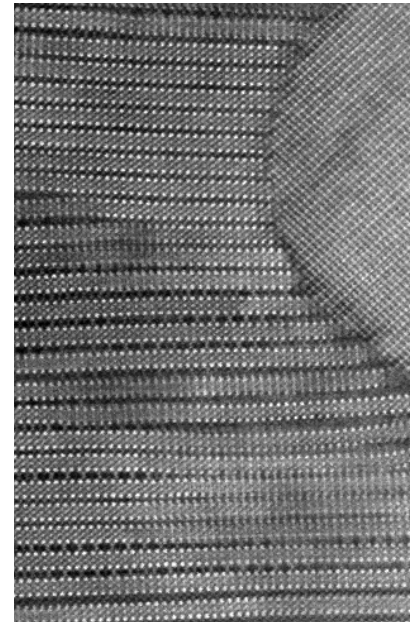
Atomic scale defects (<1 nm) demonstrated

Cu – O vacancies within Y248 intergrowth
→ weak pinning ??

Avoids the Stoichiometry Catastrophe



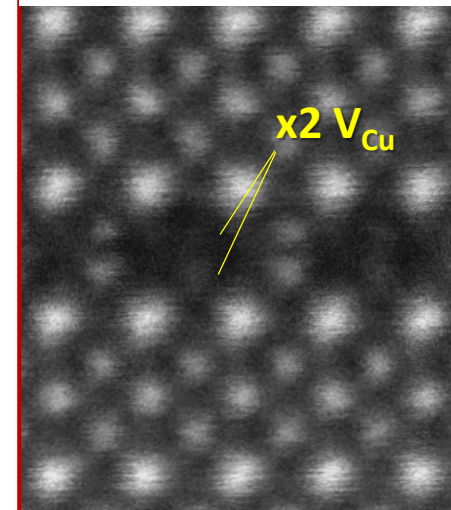
YBCO + BaZrO₃



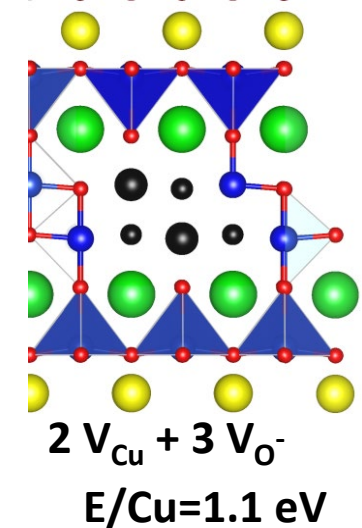
Cluster with ferromagnetism confirmed by XMCD synchrotron radiation

J. Gázquez et al, Adv. Science 3, 1500295 (2016)
E. Bartolomé et al., ACS Appl. Nano Mater. (2020)

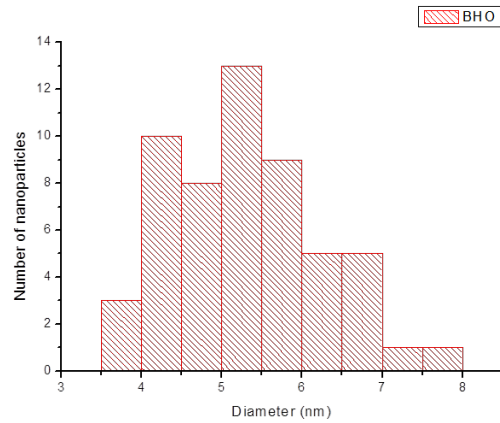
Faulted Y248



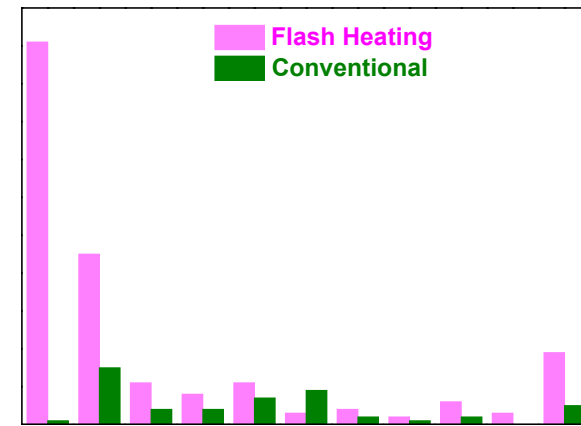
DFT calculations



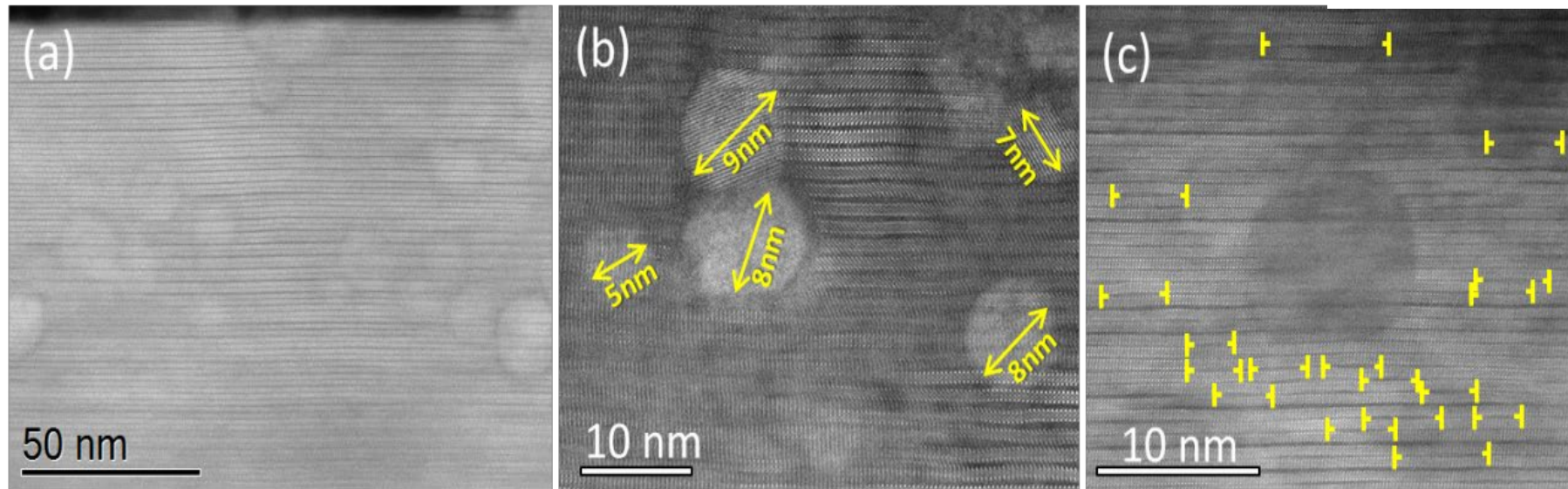
TFA-BHO pn-nanocomposites by Flash Heating



Distribution of initial NP: 4-6 nm



Flash heating (20 °C/s): 20%M BHO (5 nm)



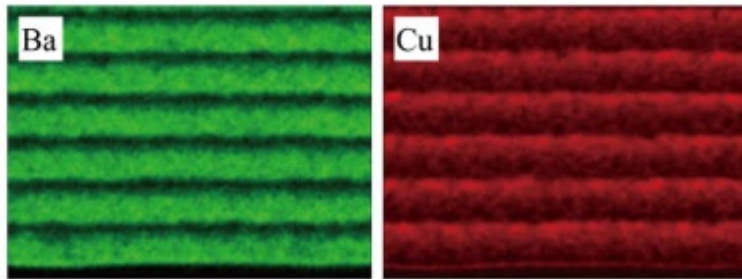
$n_{np} \approx 40 \times 10^{22} \text{ m}^{-3}$ (x2,5) ($\approx 8 \%$ vol)
 NPs random fraction: 94%

Short SFs are promoted ! (20 – 30 nm)
 Vol density partial dislocation: $\approx 2.3 \%$ vol

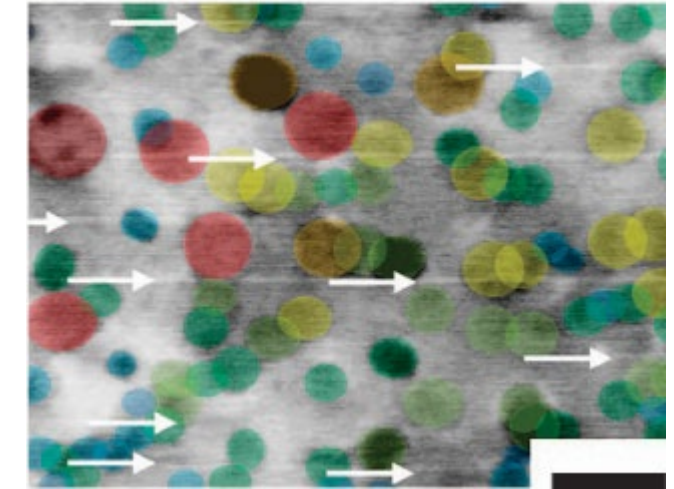
- Flash Heating strongly avoids NP coarsening
- Higher concentration of short SFs: higher density of partial dislocations
- NP size very close to the optimal size for vortex pinning (5-8 nm)

Z. Li et al, Sci Rep. (2019)
J Mat Chem C (2019)

UltraThin Once Coating (UTOOC): a route to small NPs



Multideposition with ultrathin repetition thickness (30 nm): CuO layers at the interfaces!



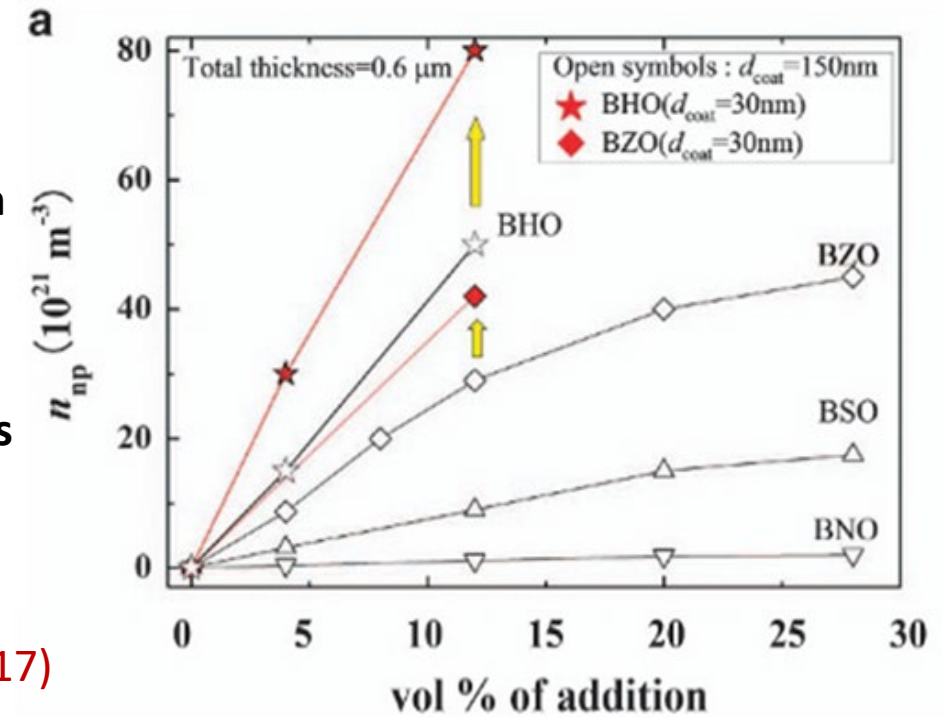
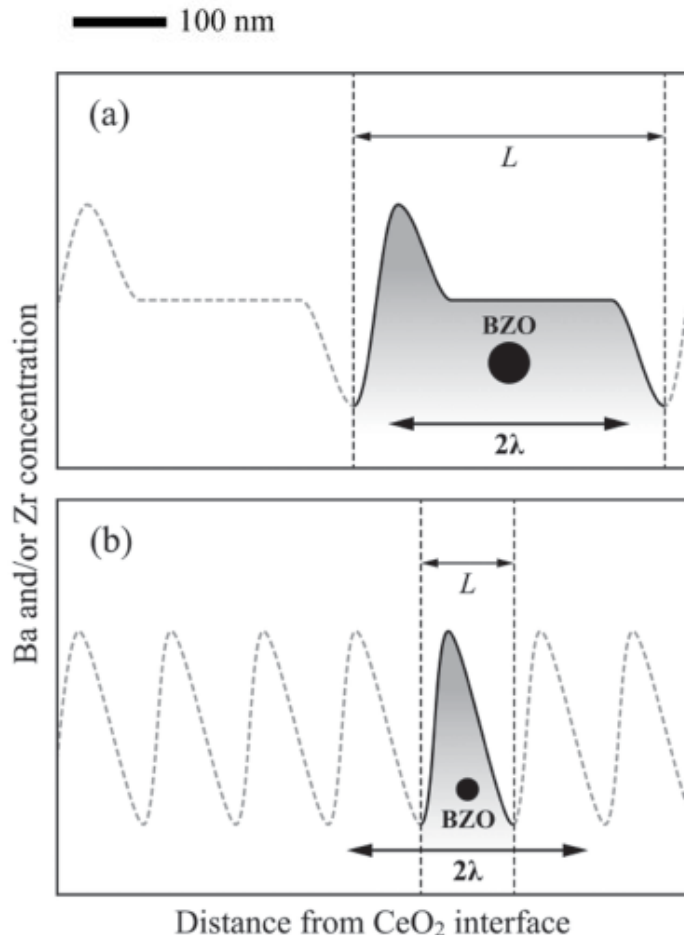
(Y,Gd)Ba_{1.5}Cu₃O_x

~ 7 nm BHO NPs

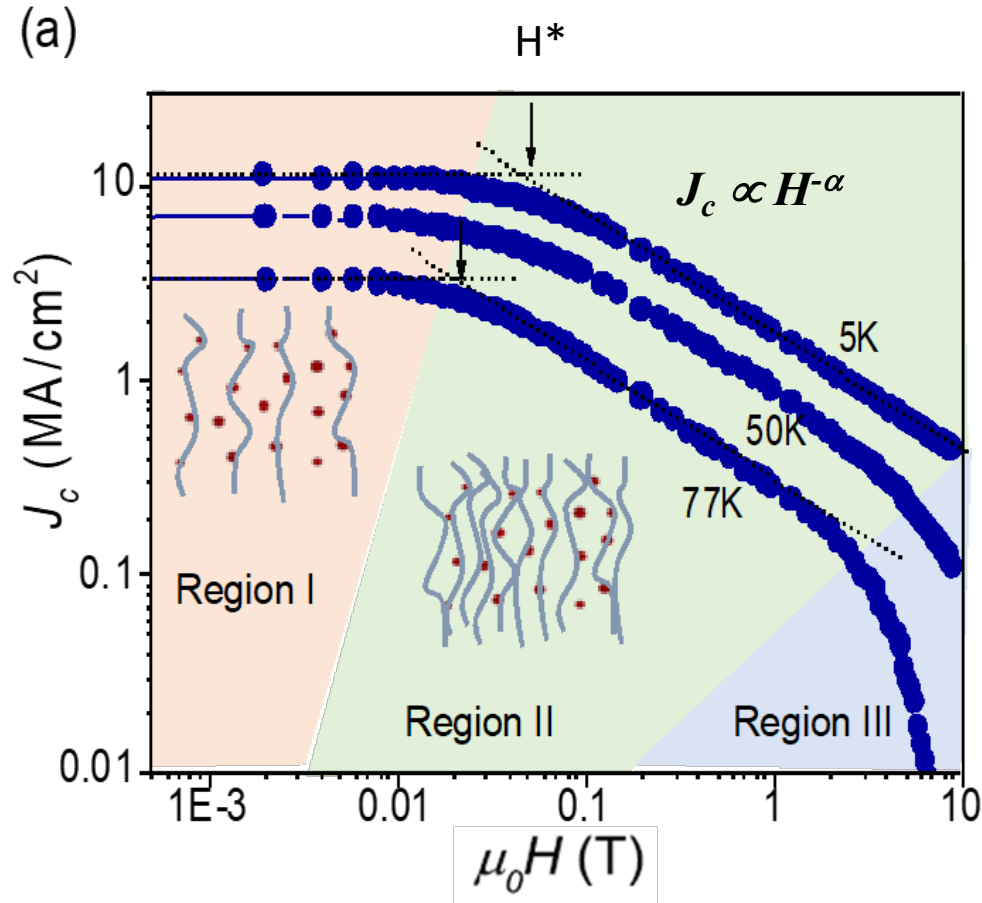
BZO and BHO nanoparticles are confined due to CuO barriers at the interface: coarsening is limited

Very high concentration of small and dispersed NPs
Volume similar to the optimal in simultaneous growth approach

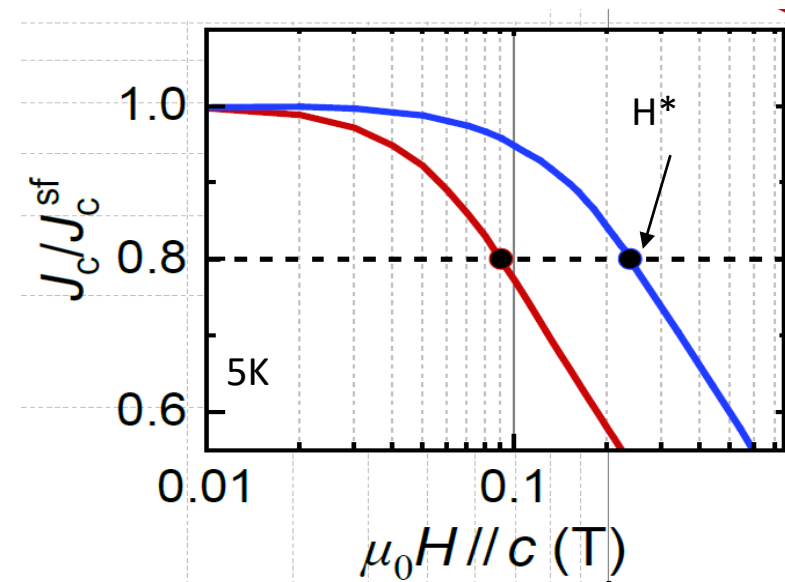
T. Izumi et al., SUST (2018)
M. Miura et al., NPG Asia Materials (2017)



Magnetic field dependence of $J_c(B,T)$: single vortex to collective pinning



- Region I: **single vortex pinning** (H^*)
- Region II: **collective vortex pinning**
- Region III: **thermal activation effects** very relevant (close to $H_{irr}(T)$)



H^* : single vortex regime (*measure of the density of pinning centers*)

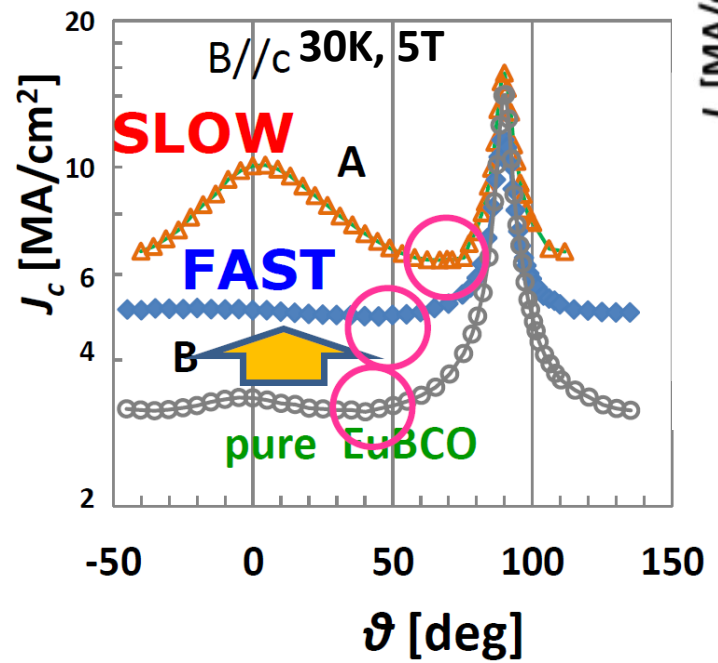
Accommodation magnetic field $H^*(T)$: very useful parameter to monitor efficiency and concentration of APCs

A decrease of α values when the nanoparticle concentration is increased (enhanced vortex pinning)

Vortex pinning consequences at high growth rate: PLD-HR

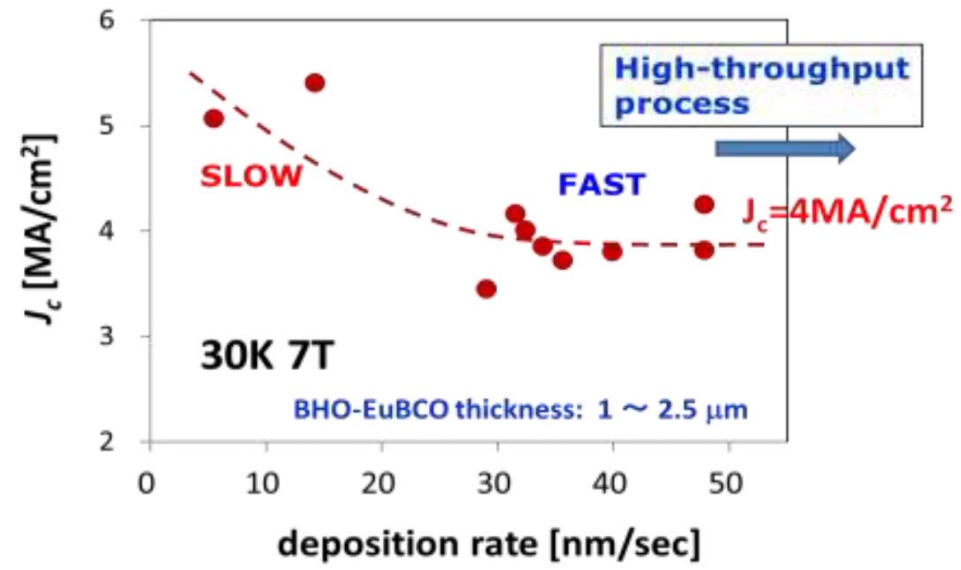


EuBCO + HfBaO₃ nanorods

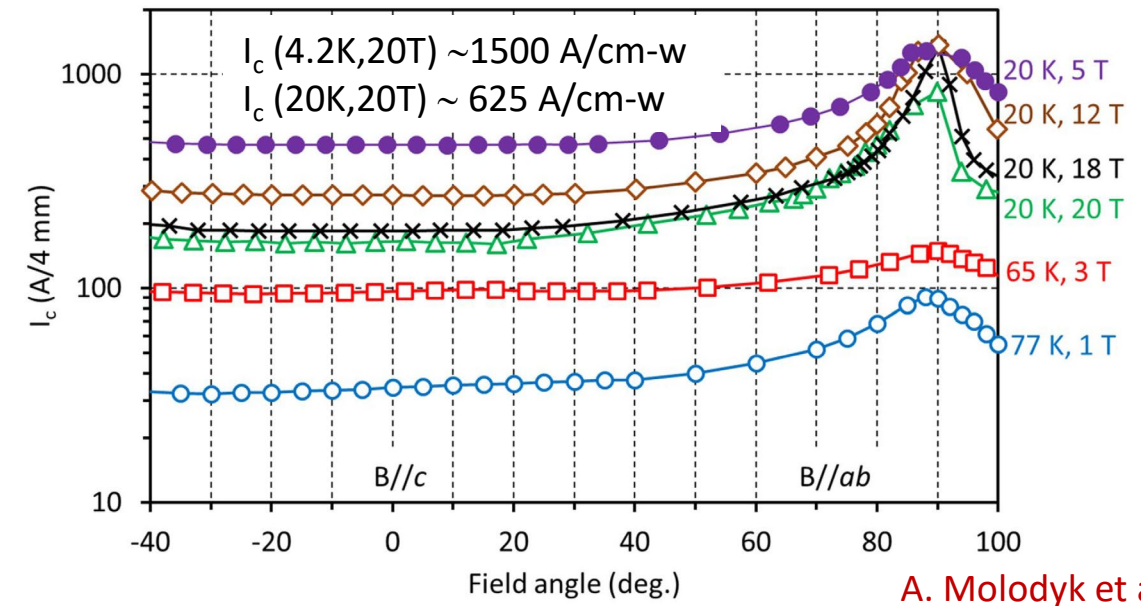
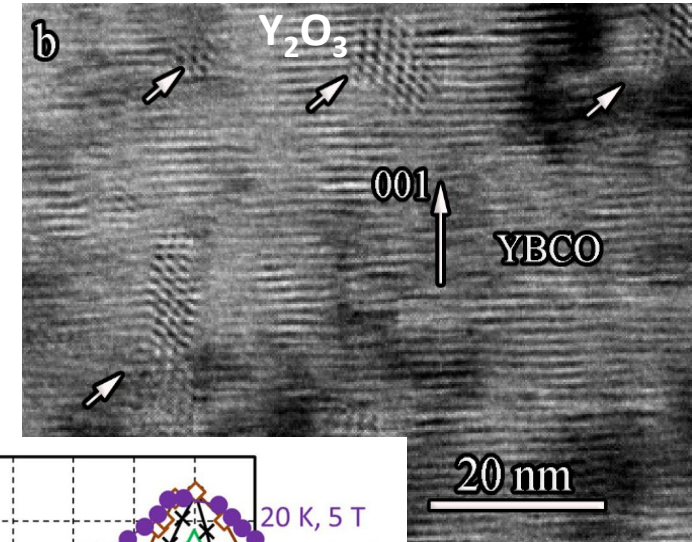


Y. Iijima, CCA 2023

Aligned long nanorods are not essential at low T - high H

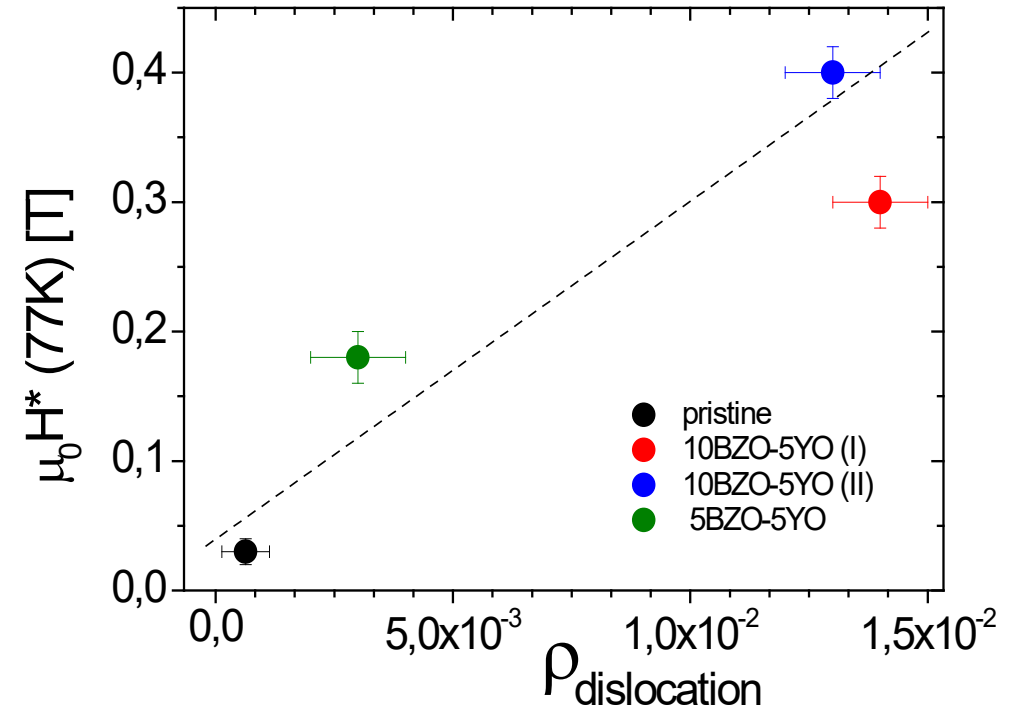
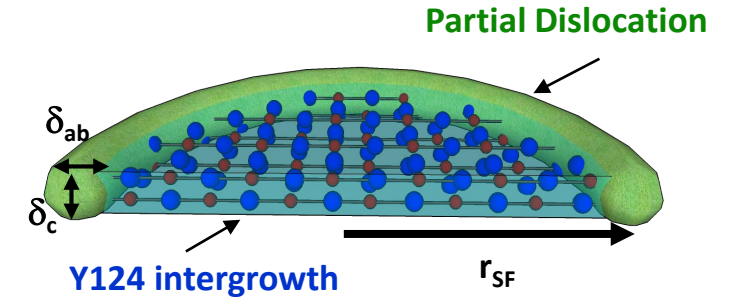
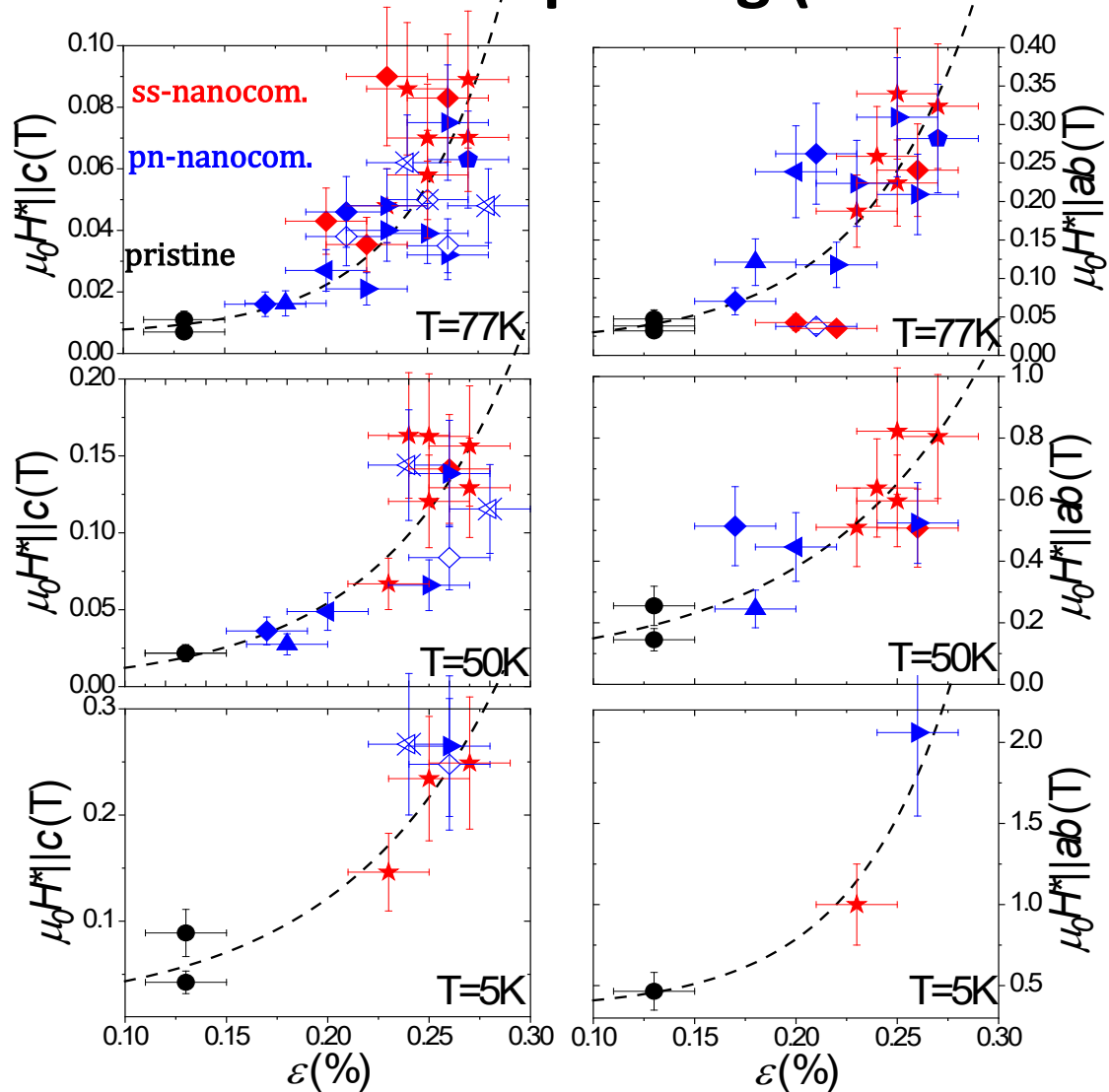


YBCO + Y₂O₃ nanoparticles



A. Molodyk et al, Sci. Rep 11 (2021)

Nanostrain is the most relevant parameter controlling single vortex pinning (CSD-TFA and CSD-TLAG)



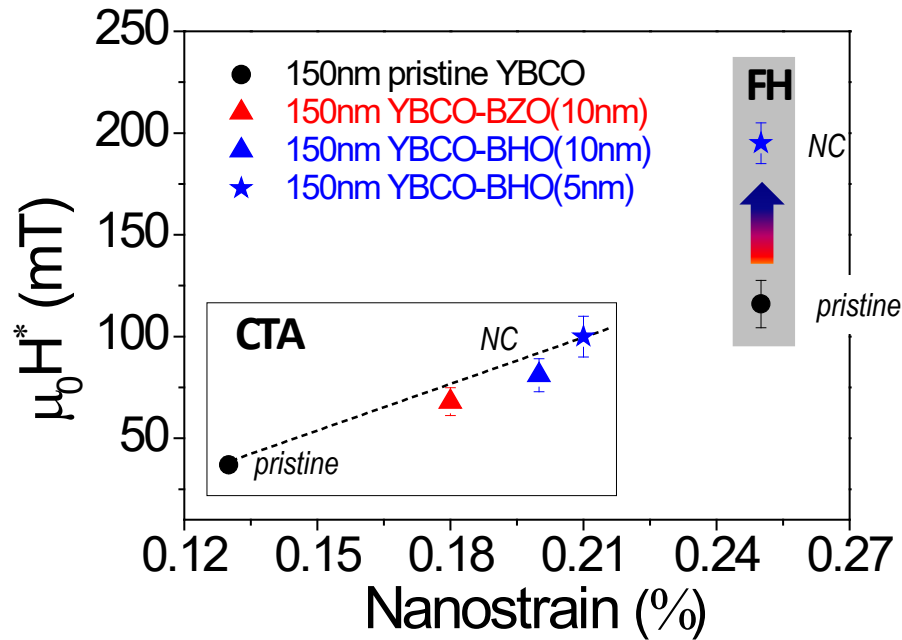
**H^* enhanced by nanostrain
 $H//c$ and $H//ab$**

F. Vallés et al, *Comm Mat* 3,45 (2022)
Z. Li et al., *Sci Rep* (2019)

**Close relationship among dislocation
density and nanostrain**

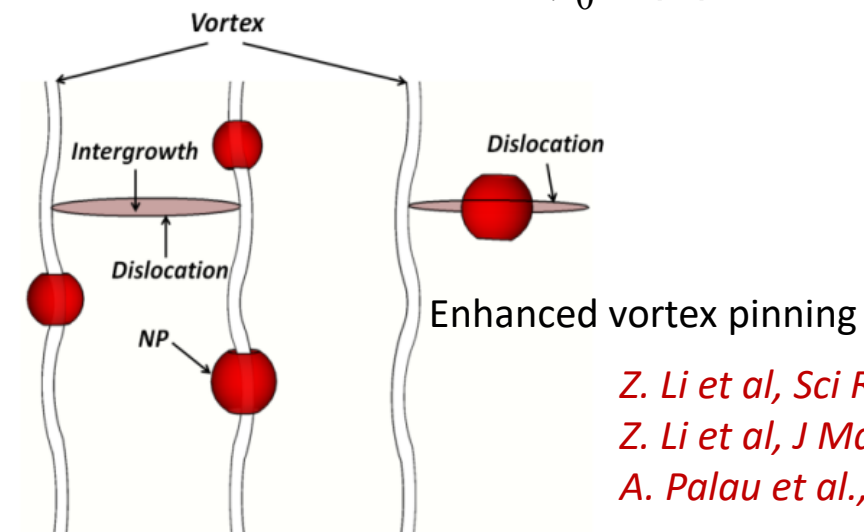
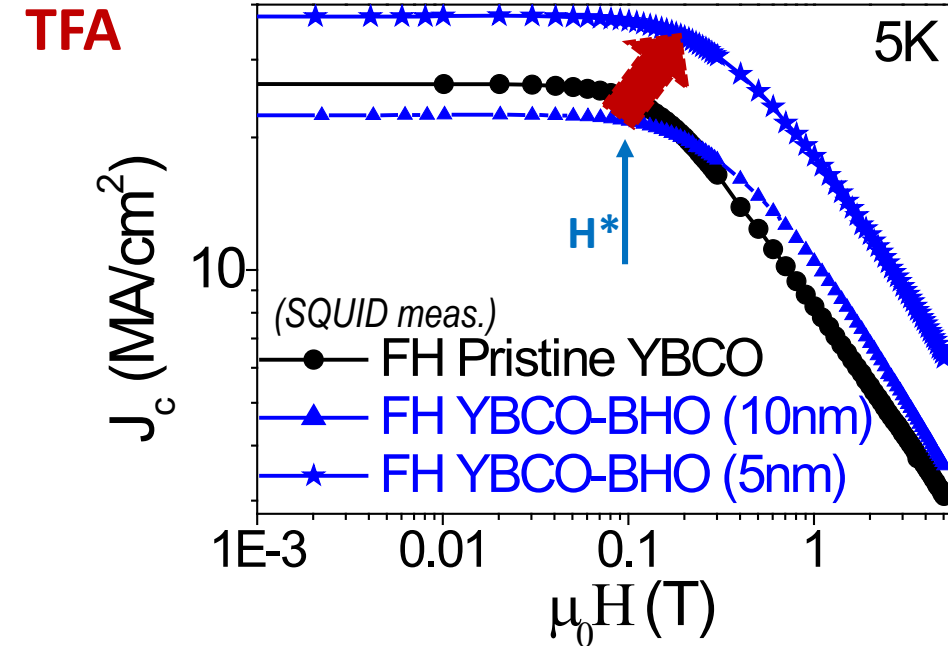
Synergistic combination of Nps and nanostrain: enhanced vortex pinning

CTA: Conventional Thermal Annealing (0.4 °C/s)
FH: Flash heating (20°C/s) - Enhanced vortex pinning



A leap increase of H^* beyond nanostrain
 NP diameter $\sim \xi_{ab}$ (coherence length)

Nanostrain & NPs (4-8 nm): Synergistic effect for enhanced vortex pinning

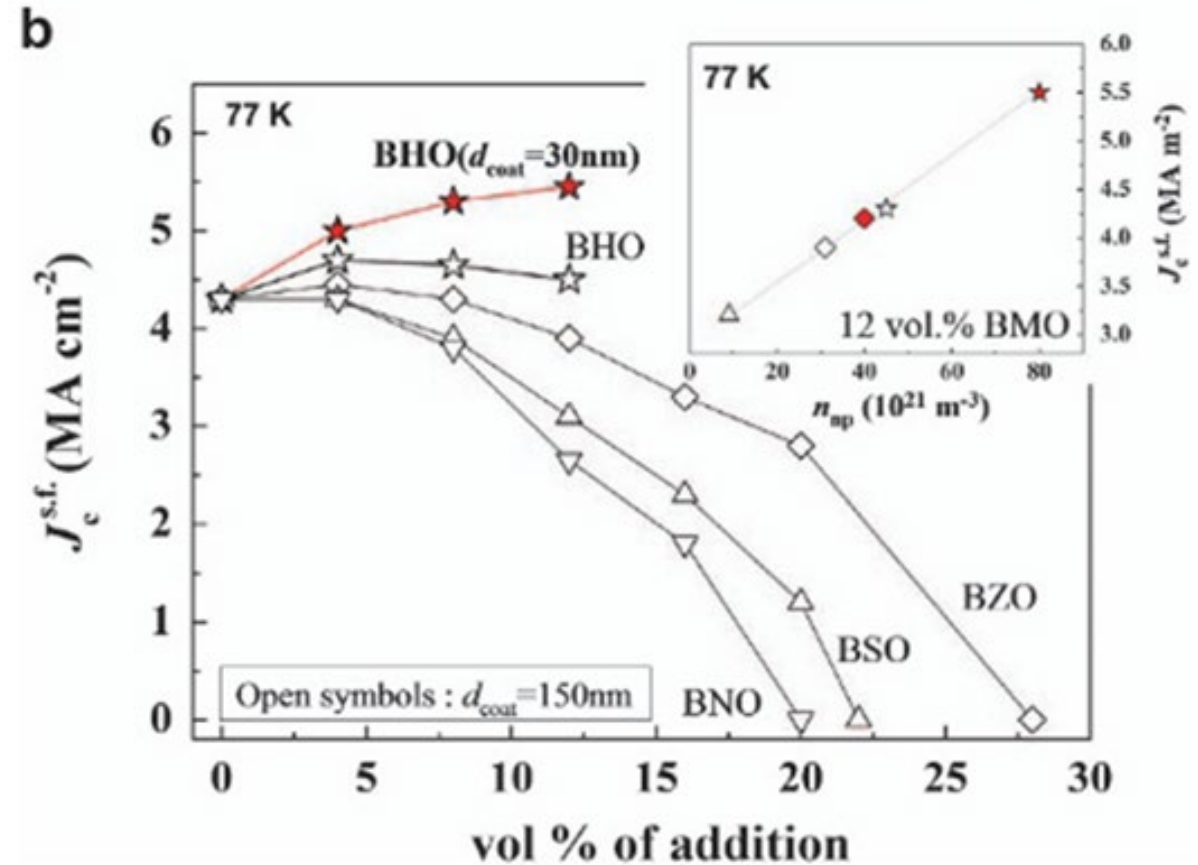
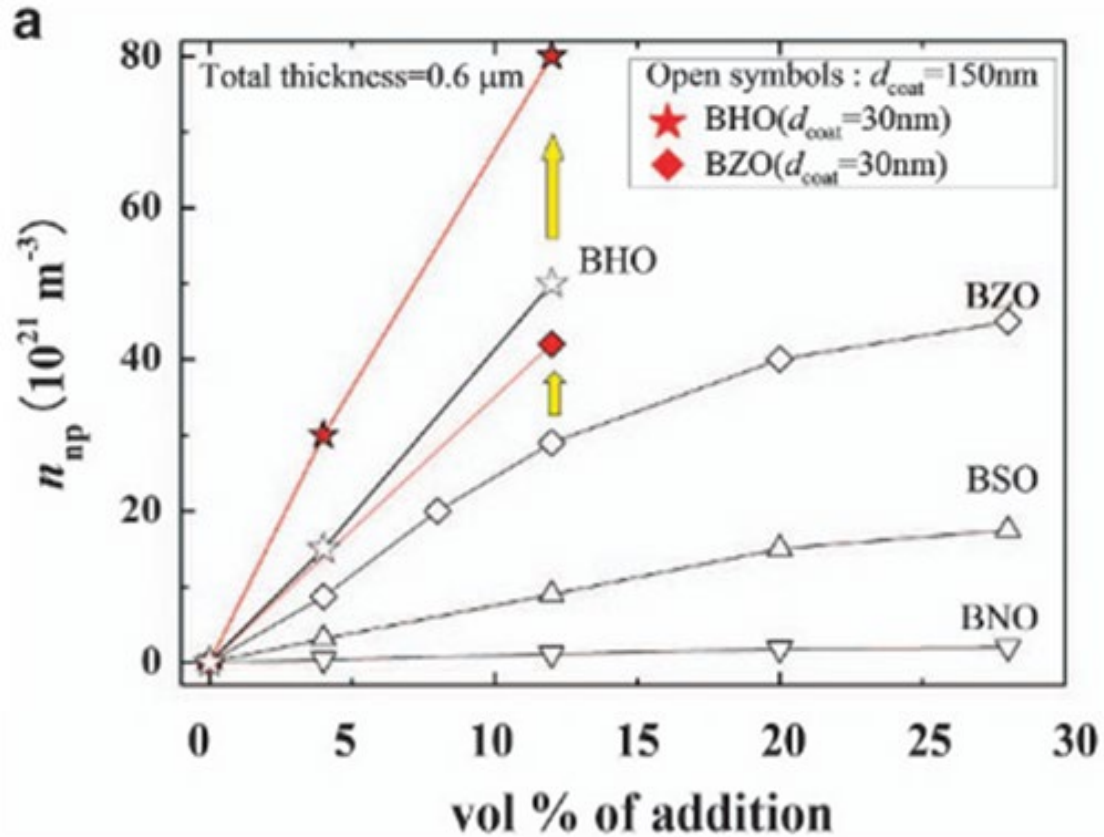


Z. Li et al, *Sci Rep.* (2019)
 Z. Li et al, *J Mat Chem C* (2019)
 A. Palau et al., *SUST* (2018)

Enhanced vortex pinning by nanoparticles (UTOOC)

CSD-TFA growth: (Y,Gd)Ba_{1.5}Cu₃O_x / BHO

$$J_{CO}^{NPs} \propto N_{np} \frac{\mu_0 H_c^2 \pi \xi^2 D}{4\xi} \propto N_{np} \left(\frac{1}{\lambda^2 \xi} \right)$$



Very small BHO NPS achieved with UTOC (~ 7 nm)
with coatings of 30 nm

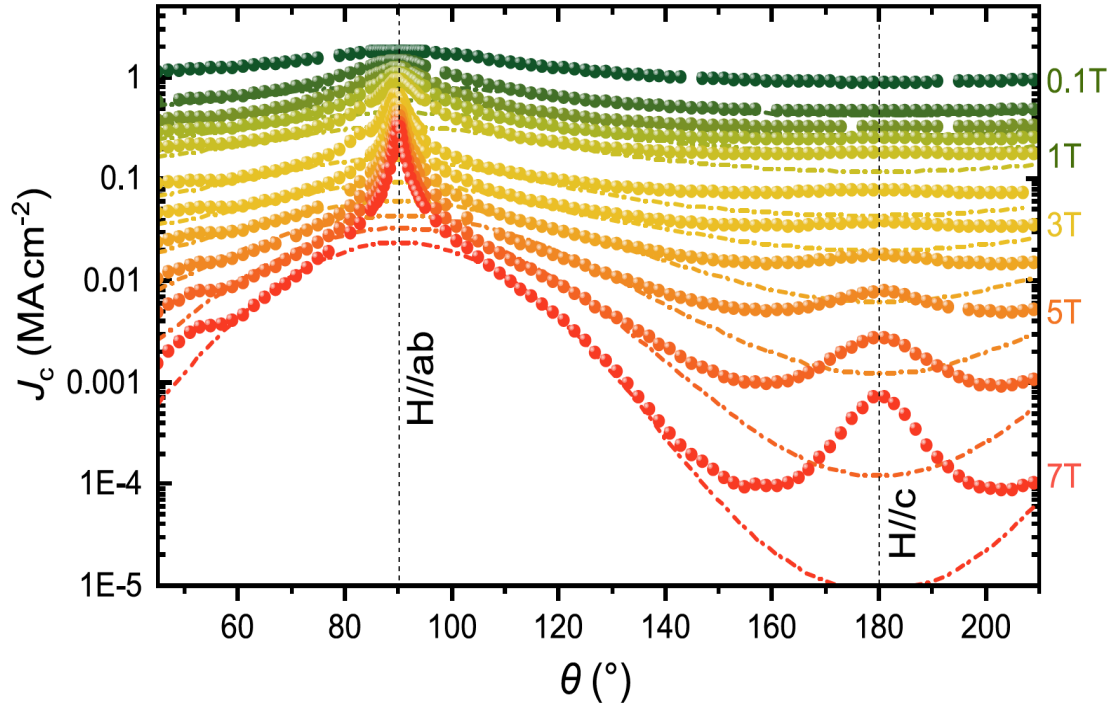
Very small BHO NPs contribute as APCs

M. Miura et al., NPG Asia Materials (2017)

Anisotropy of superconducting properties

Effective anisotropy decrease due to nanostrain (SFs) and nanoparticles

$$\epsilon_{\text{eff}}(\theta) = [\cos^2\theta + \gamma_{\text{eff}}^{-2}\sin^2\theta]^{1/2}$$



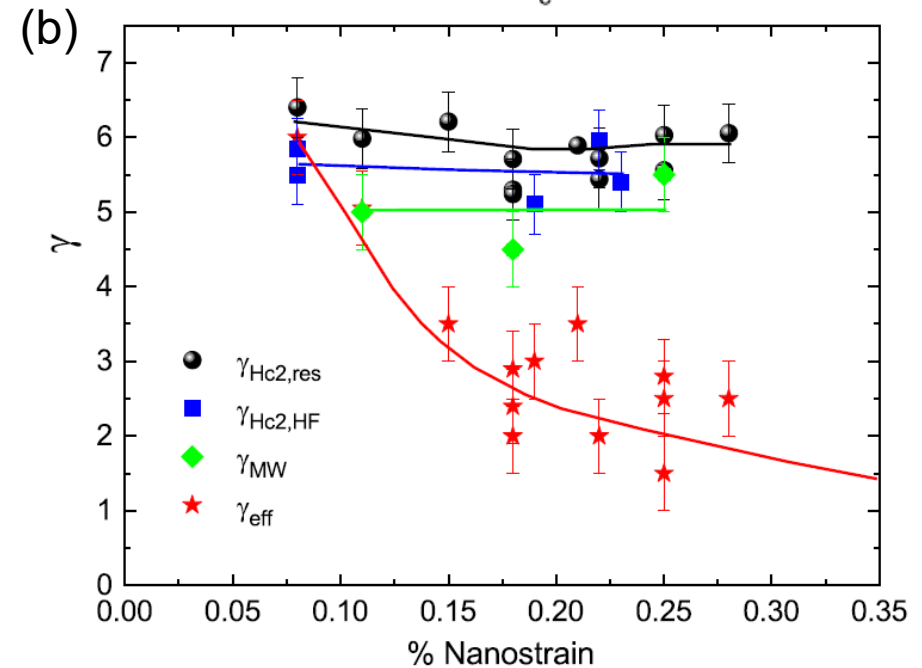
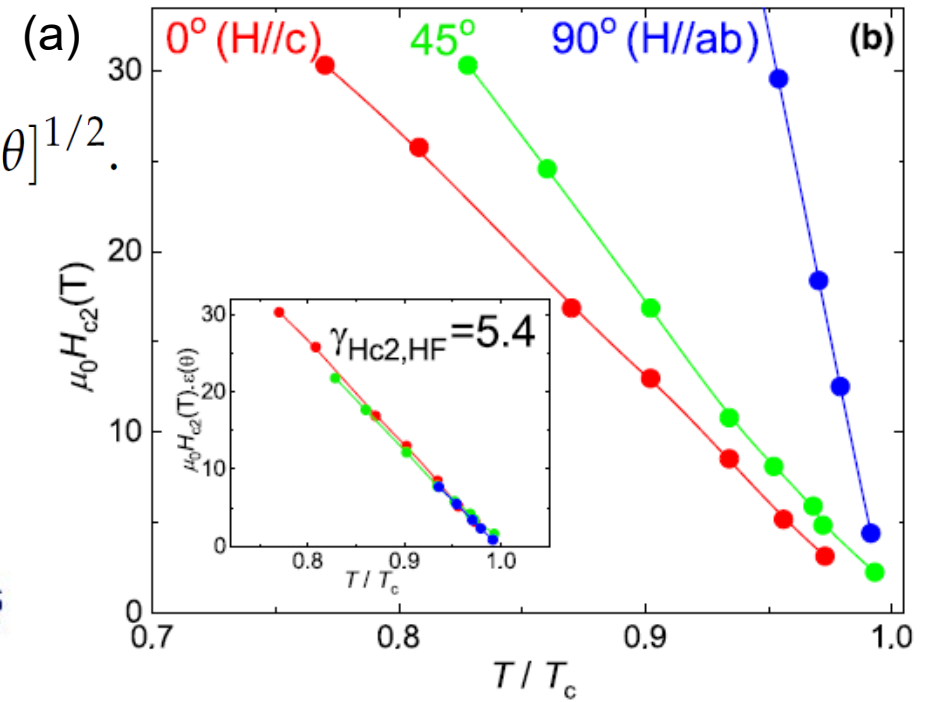
Isotropic and anisotropic pinning contributions

L. Soler et al, Nature Communications (2020)

E. Bartolomé et al., Phys Rev B (2019)

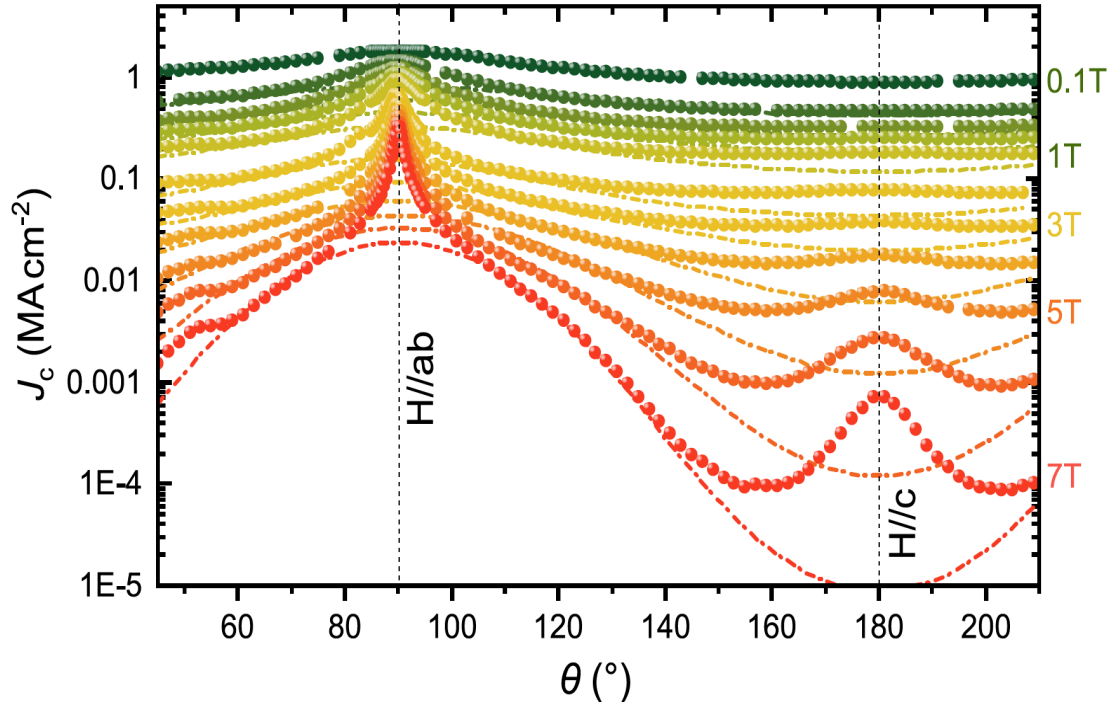
N. Pompeo et al., SUST (2020)

J. Banchewski et al, to be published

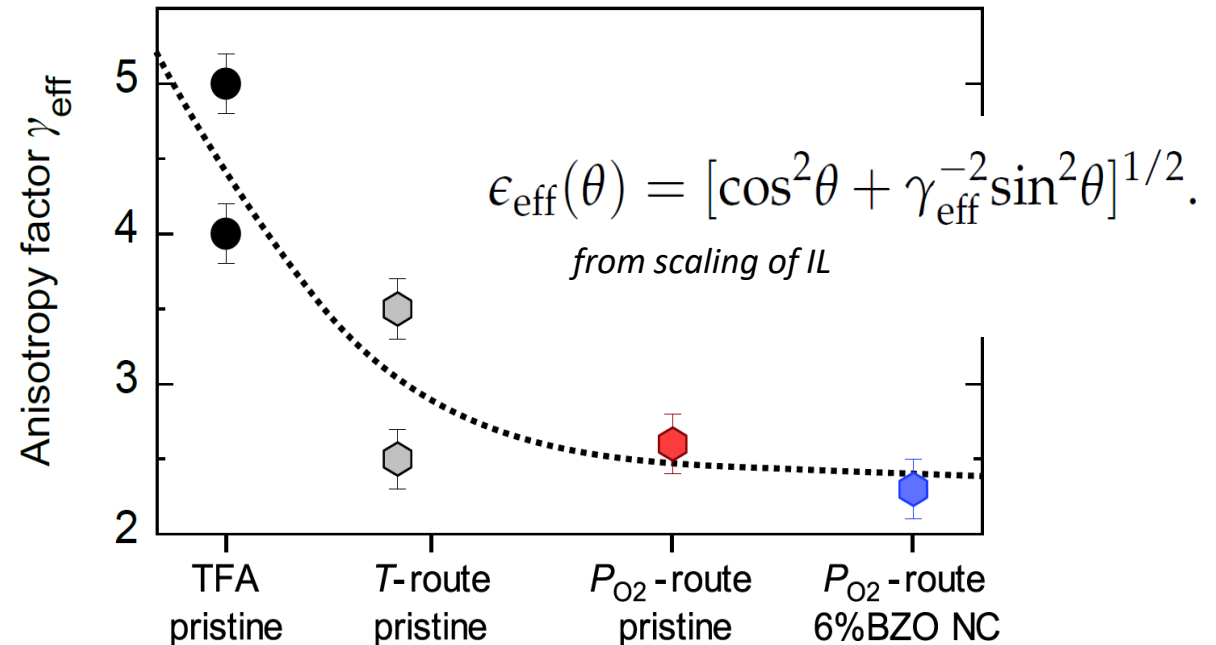


Anisotropy of superconducting properties

Effective anisotropy decrease due to nanostrain (SFs) and nanoparticles



Isotropic and anisotropic pinning contributions



L. Soler et al, Nature Communications (2020)

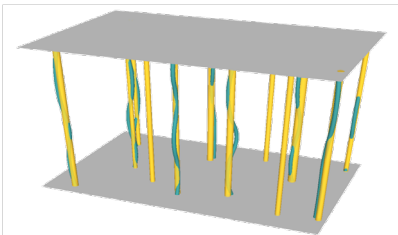
E. Bartolomé et al., Phys Rev B (2019)

N. Pompeo et al., SUST (2020)

J. Banchewski et al, to be published

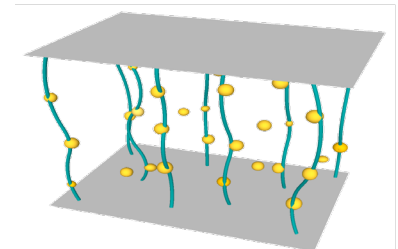
Strong/Weak Vortex Pinning Contributions: temperature dependence

$$J_c(T) = J_c^{\text{iso-wk}}(T) + J_c^{\text{iso-str}}(T) + J_c^{\text{aniso-str}}(T)$$



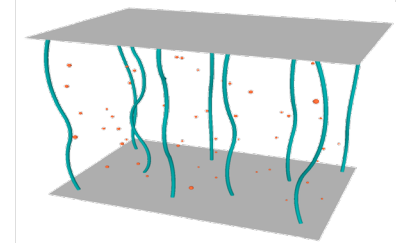
Anisotropic strong

- Nanorods (H//c)
- Intrinsic Pinning (H//ab)
- Stacking faults (H//ab)
- Twin boundaries (H//c)



Isotropic strong

- Nano-strain
- Nanoparticles



Isotropic weak

- Point defects, Oxygen and cationic vacancies

$$J_c^{\text{strong}}(T) = J_c^{\text{str}}(0) \exp \left[-3 \left(\frac{T}{T^*} \right)^2 \right]$$

$J_c^{\text{str}}(0) \rightarrow$ density of strong defects

$T^* \rightarrow$ characteristic vortex pinning energy of strong defects

$$J_c^{\text{weak}}(T) = J_c^{\text{wk}}(0) \exp \left(-\frac{T}{T_0} \right)$$

$J_c^{\text{wk}}(0) \rightarrow$ density of weak defects

$T_0 \rightarrow$ characteristic vortex pinning energy of weak defects

We can quantify the pinning strength and energies associated to different pinning centres

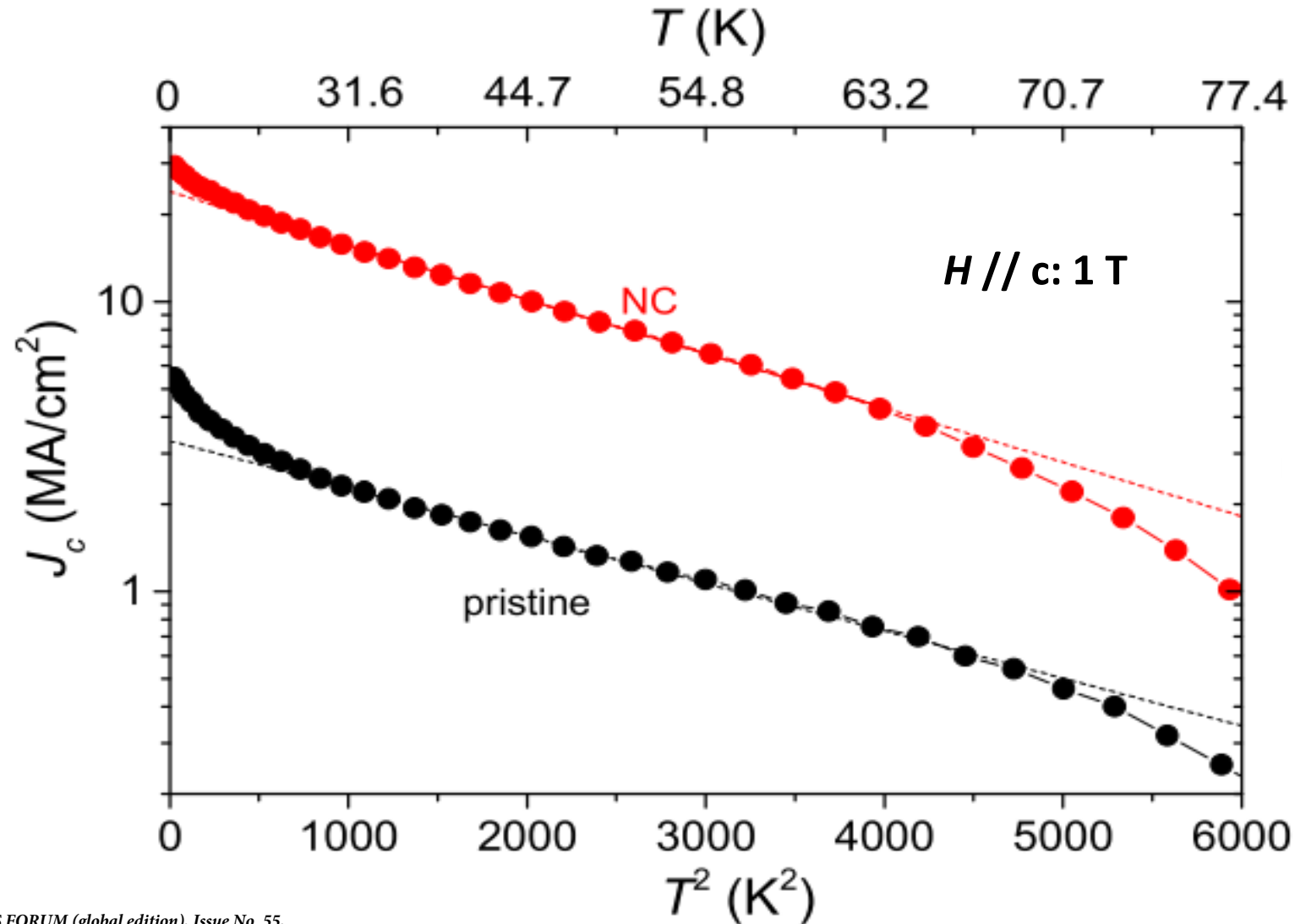
We assume additive effects of strong and weak APCs

D.R.Nelson and V.M.Vinokur: PRL, 68: 2398 (1992) ; PRB, 48: 13060 (1993)

G.Blatter.et.al., RMP, 66: 1125 (1994)

Strong/Weak/Isotropic-Anisotropic Vortex Pinning Contributions: temperature dependence

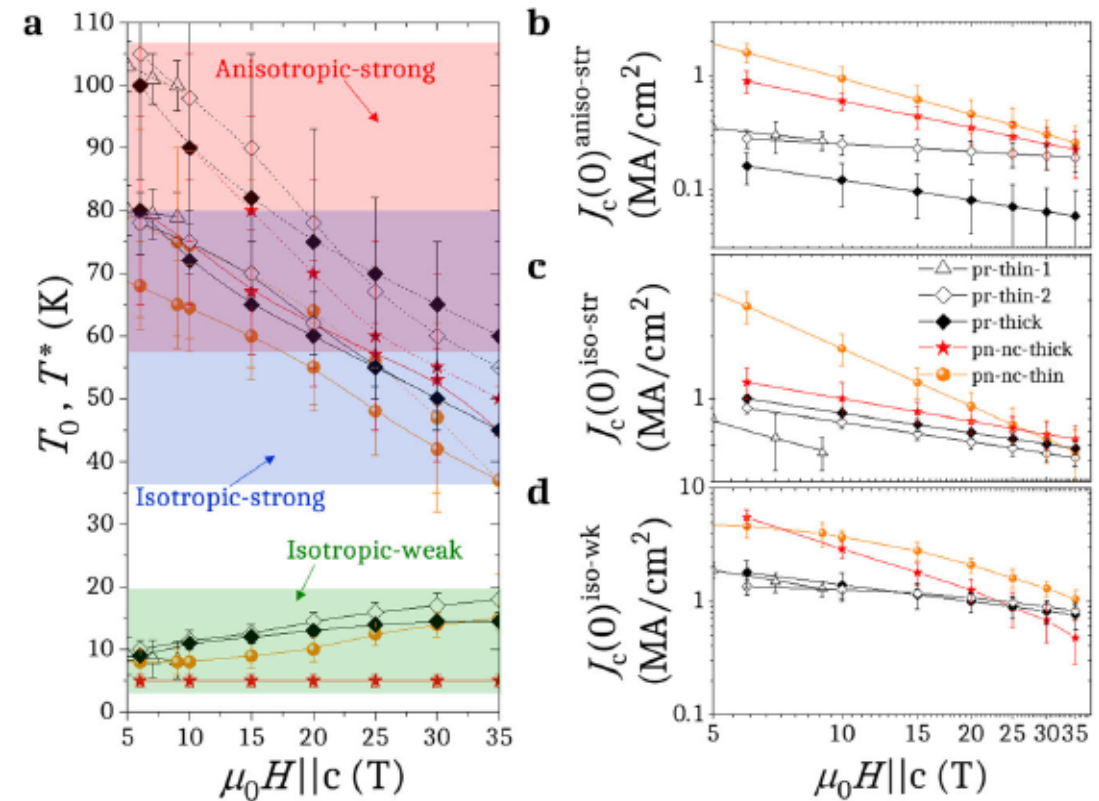
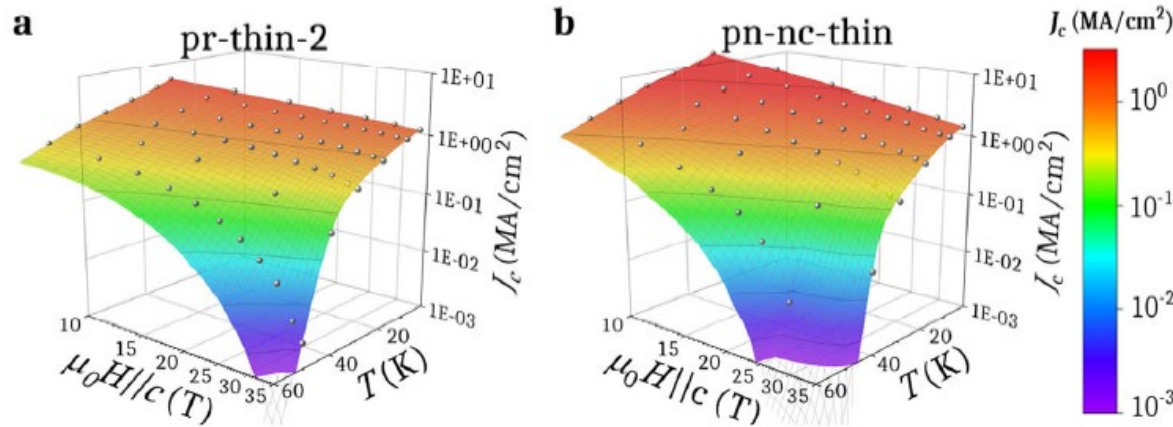
Considering the same density of defects ($J_c(0)$)



Pinning contributions in nanocomposite films: very high magnetic fields (35 T)

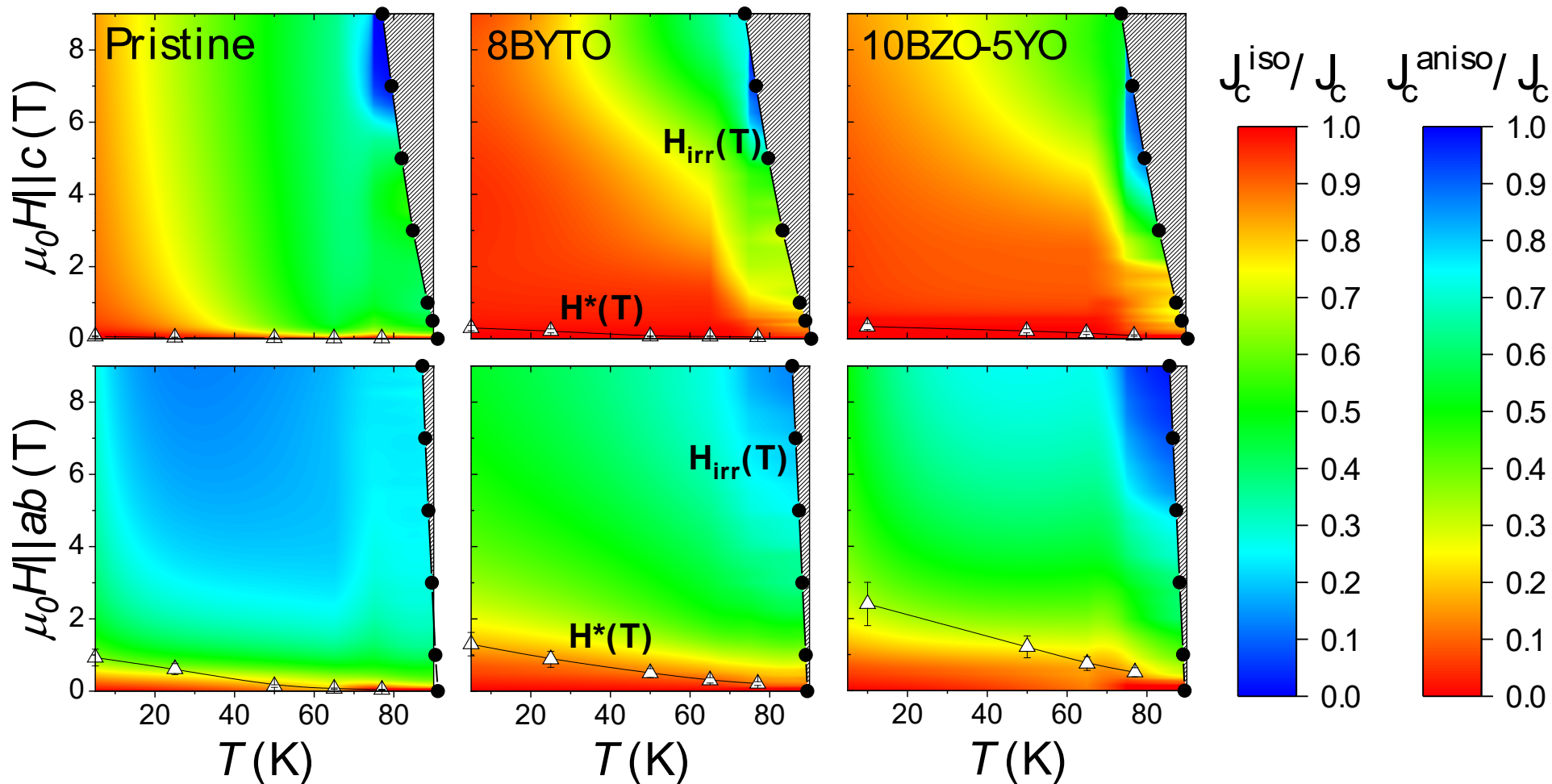
$$J_c(T) = J_c(0)^{\text{iso-wk}} \exp(-T/T_0) + J_c(0)^{\text{iso-str}} \exp(-3(T/T^*_{\text{iso-str}})^2) + J_c(0)^{\text{aniso-str}} \exp(-3(T/T^*_{\text{aniso-str}})^2)$$

D. Abraimov
 J. Jaroszynski
 D. Larbalestier



- Very different magnetic field dependences for weak and strong pinning defects
- Weak pinning defects may play a critical role at very high magnetic fields and low temperatures

Phase diagrams of vortex pinning strength

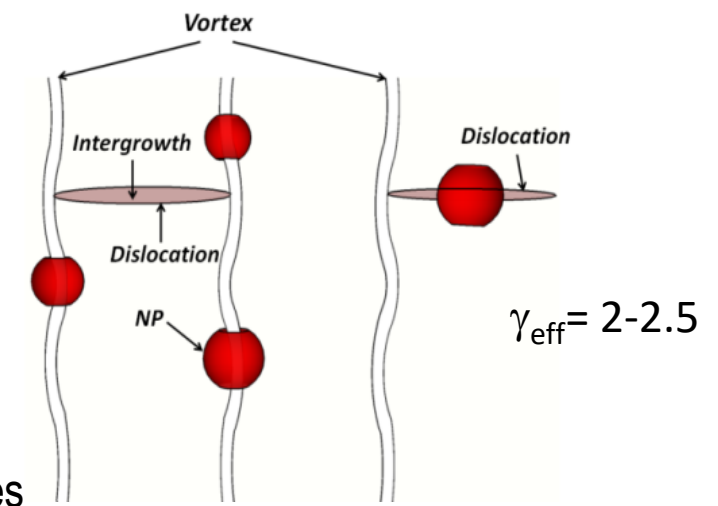
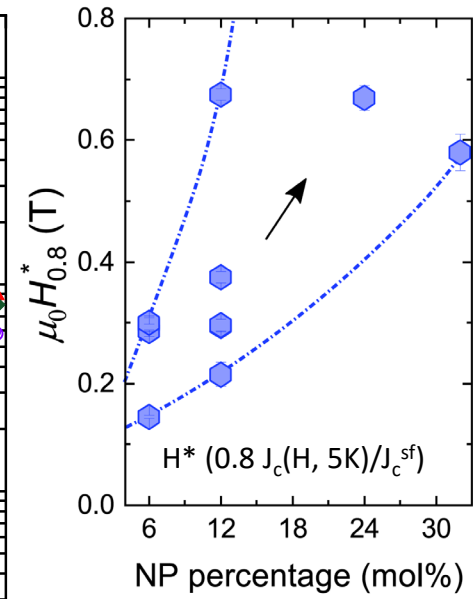
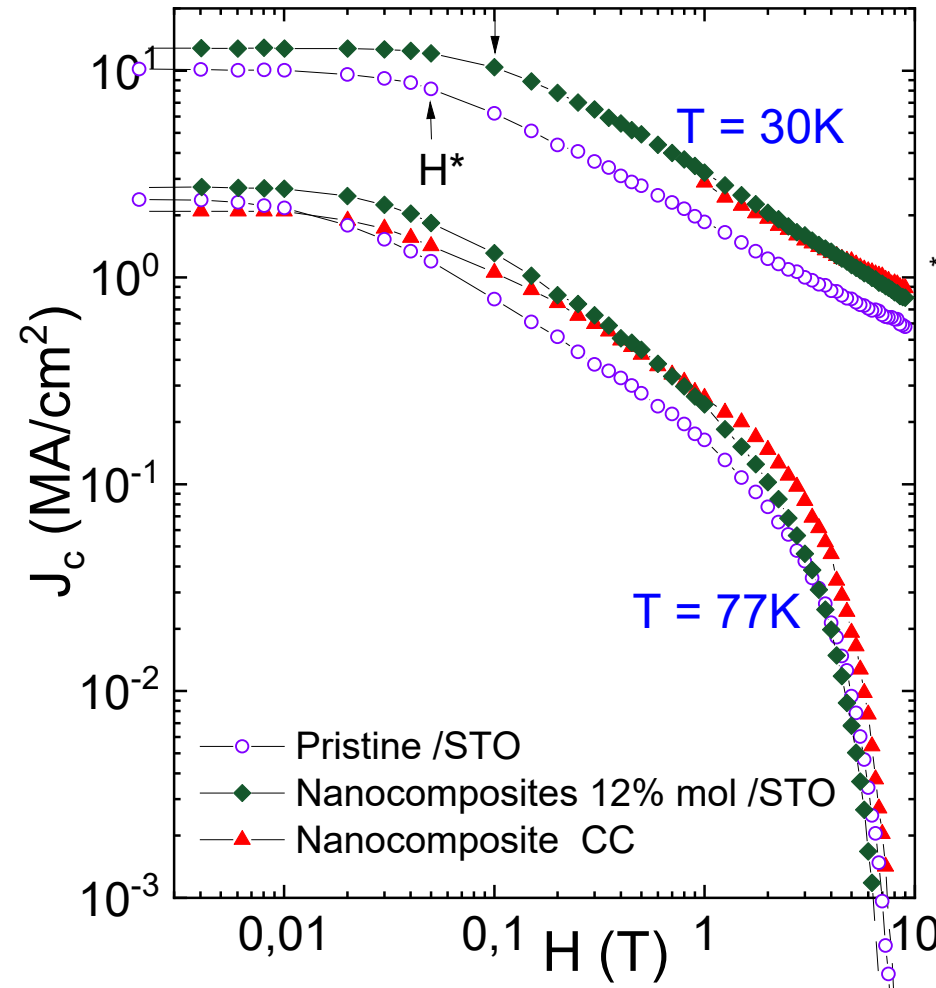
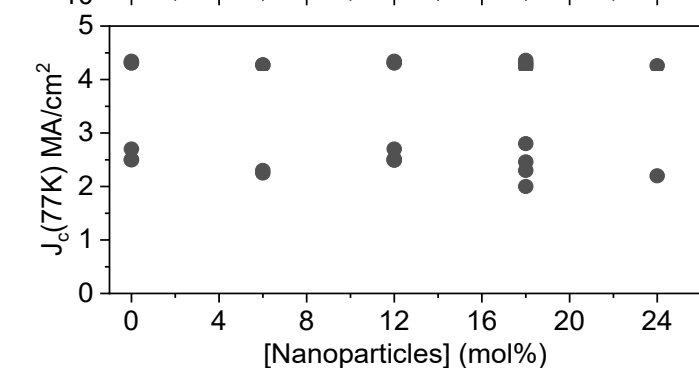
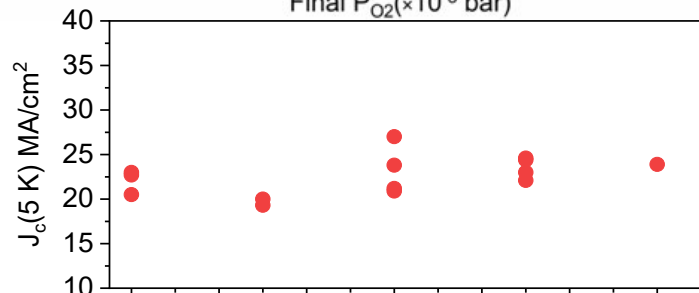
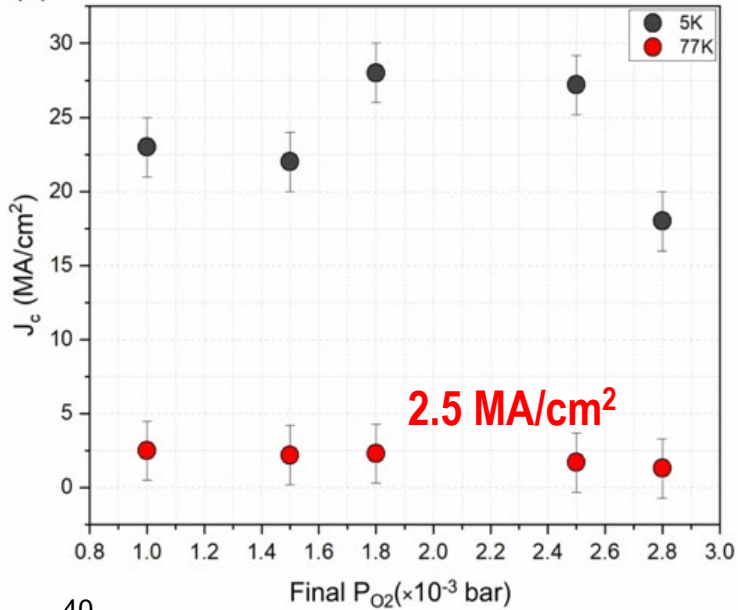


CSD nanocomposites: Single Vortex Pinning vs collective pinning

- Isotropic pinning dominates most of phase diagram ($H//c$)
- Isotropic and anisotropic pinning with similar relevance in most of the phase diagram ($H//ab$)

Vortex pinning consequences at high growth rate: TLAG-CSD

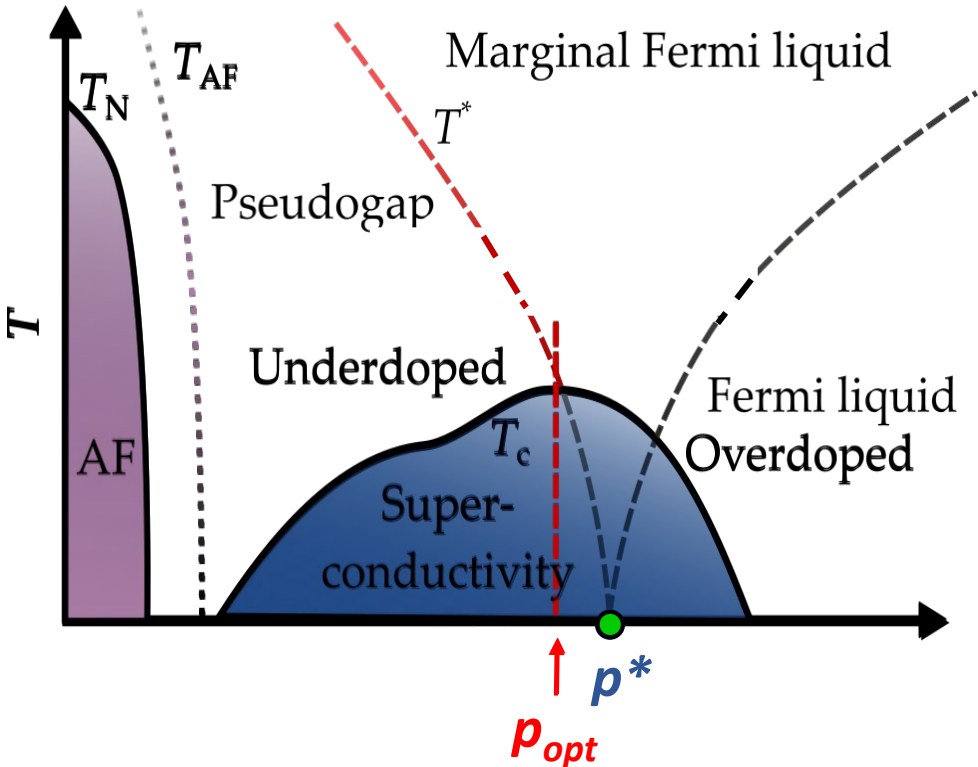
50 nm/s → 1500 nm/s



Rich vortex pinning determined by the defect microstructure of high growth rates

L. Soler et al., Nat Comm (2020), S. Rasi, et al, Advance Science (2022)

Tune charge carrier density by oxygen overdoping



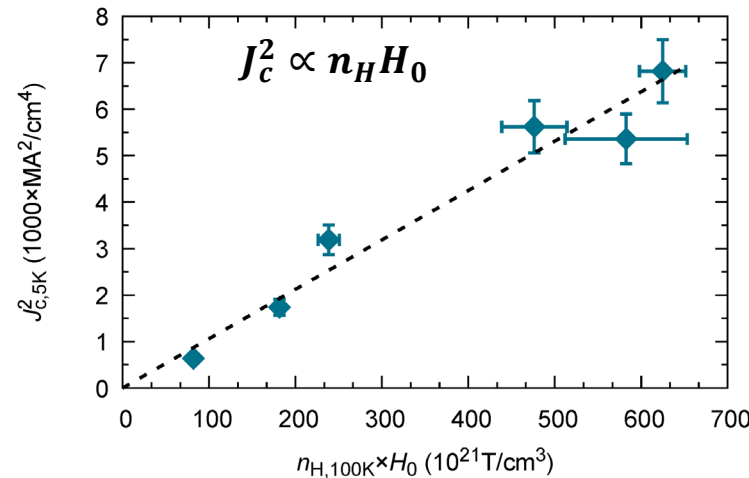
$p_{opt} = 0.16$ holes/ CuO_2 -plane: optimal doping for maximum T_c
 $p^* = 0.19$ holes/ CuO_2 -plane: Critical doping (QCP)

$$\text{Pinning force } F_p = \sum_i^{N_p} f_{p,i}(B, T) \propto J_c$$

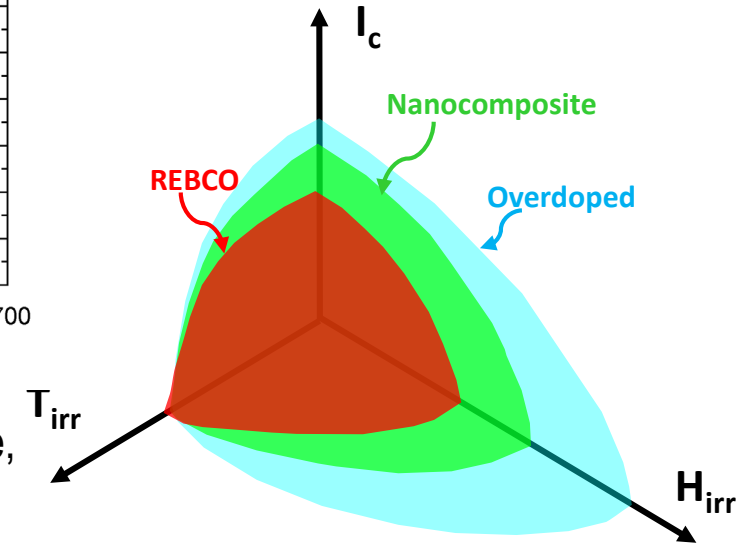
$$f_p \propto E_c \text{ condensation energy}$$

$$J_d^2 \propto n_s E_c \longrightarrow J_c^2 \propto n_H H_0 \text{ (} H_0 \text{ from in-plane magnetoresistance)}$$

(three independent experimental parameters)

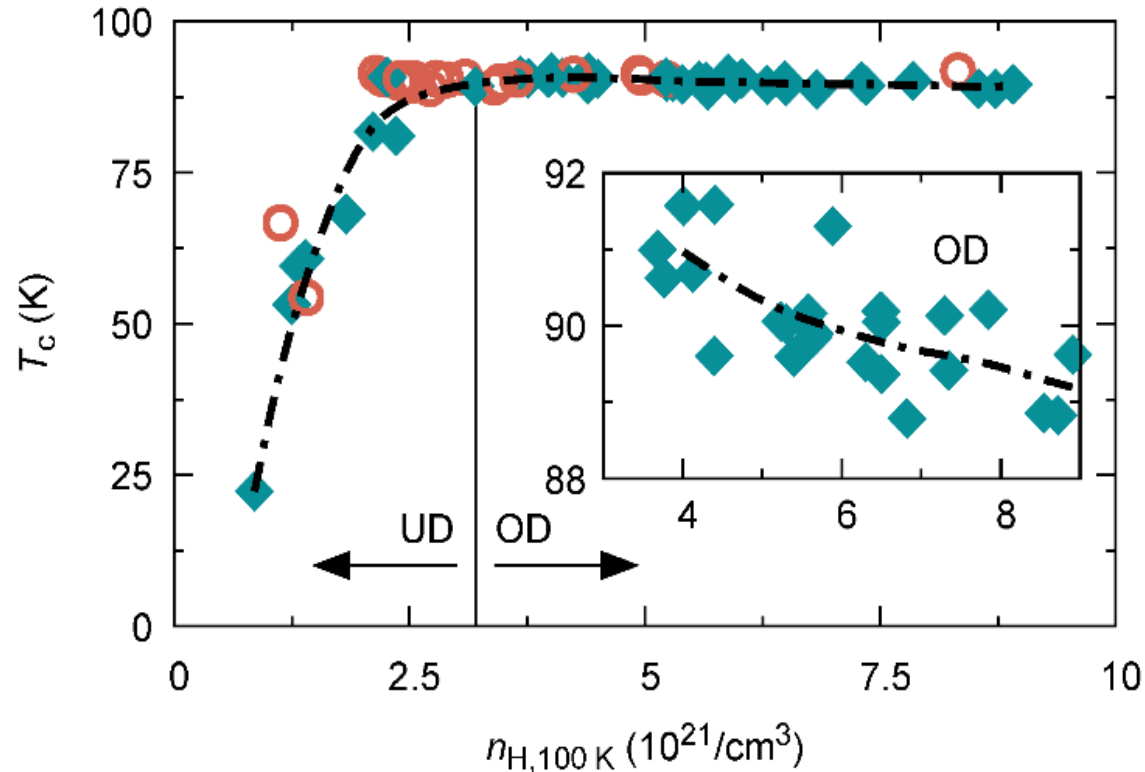


n_H and E_c increases in the overdoped state, and consequently J_c should increase

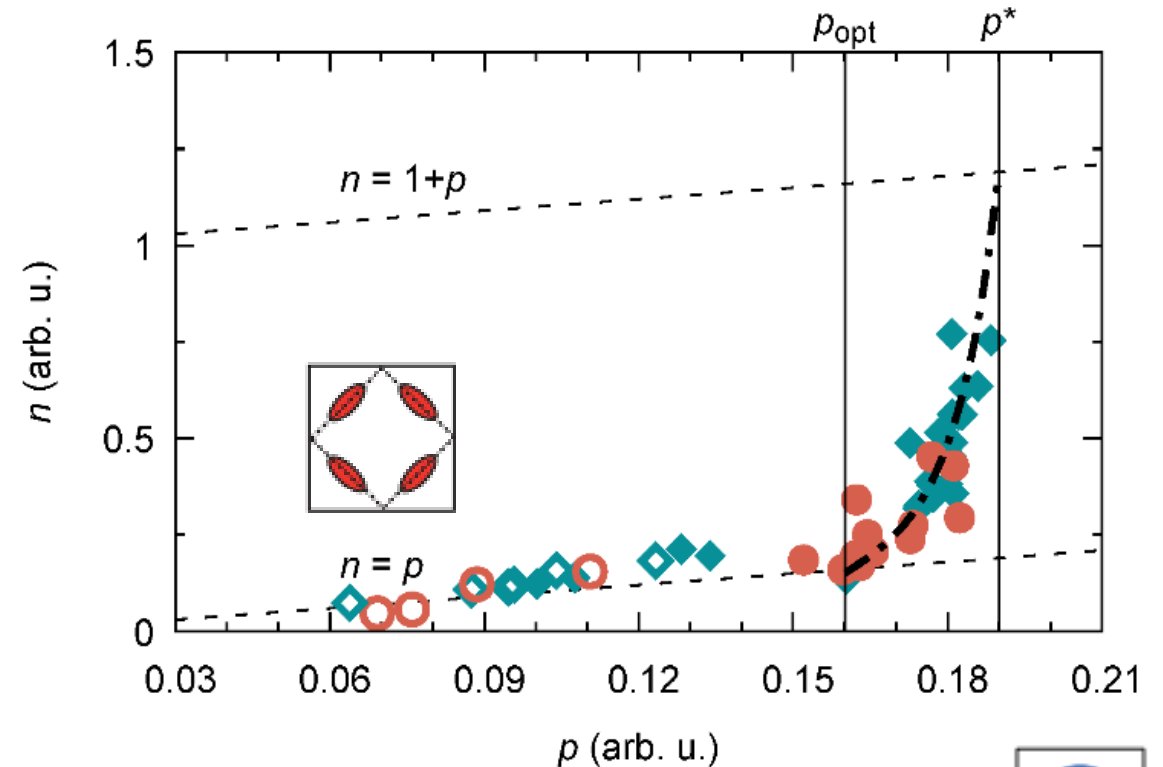


Carrier concentration effects: oxygen overdoping

YBCO PLD and TFA – CSD thin films



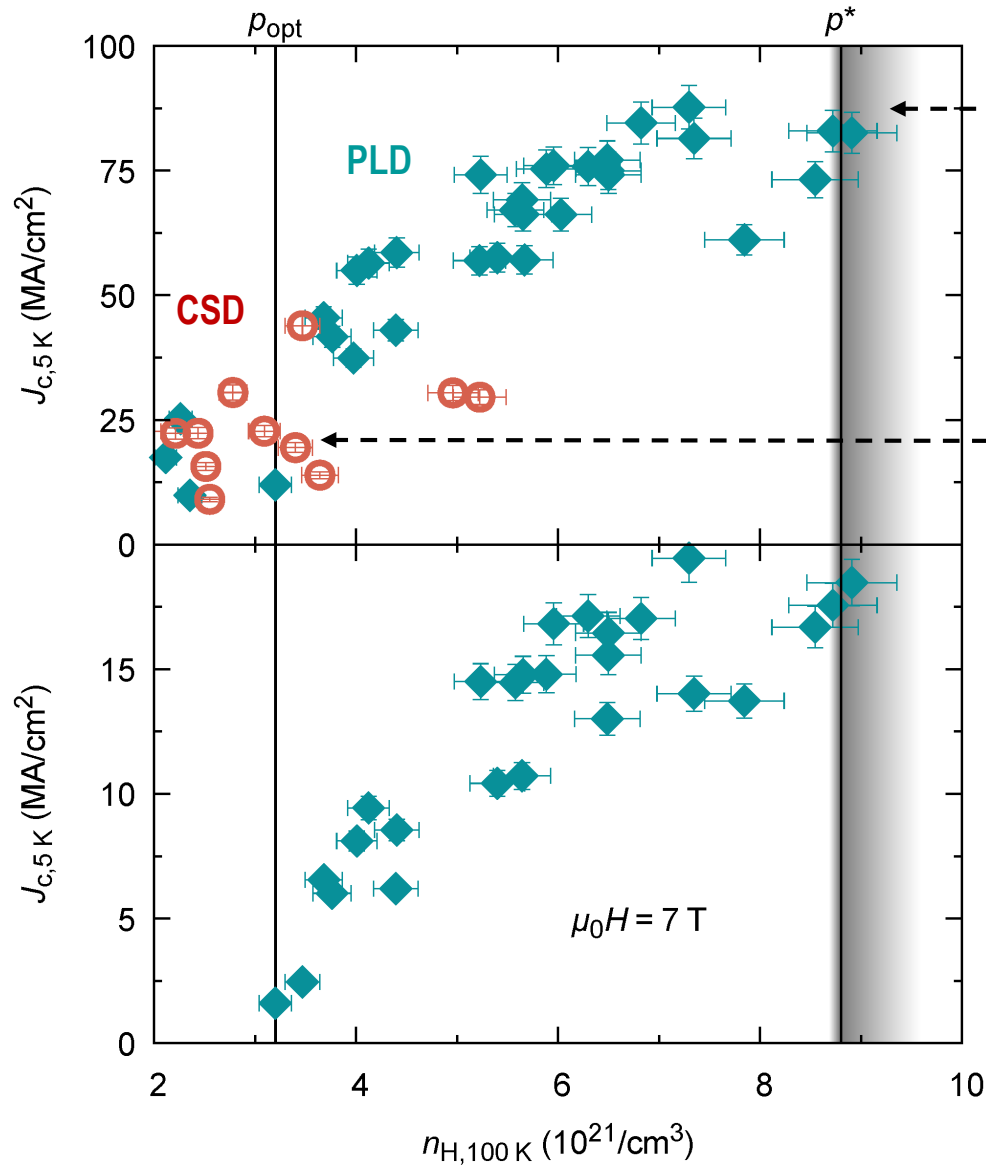
- Carrier concentration determined by Hall effect (100 K)
- Overdoping is achieved by oxygen excess



- Fermi surface reconstruction at the Quantum Critical Point ($p^* > p_{opt}$): large increase of the carrier density n (cylindrical Fermi surface)
- Non-unique relation between the charge carrier density n and doping, p .



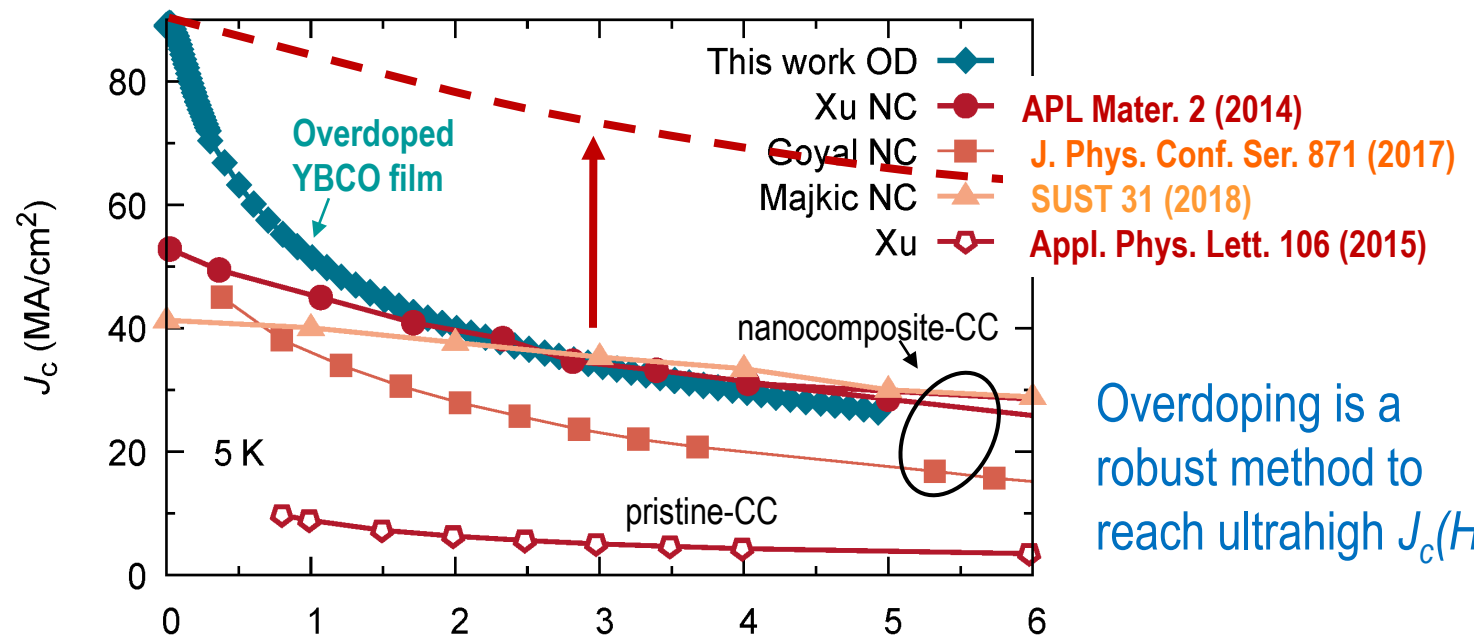
Strong increase of J_c in the overdoped state



$$J_c(p^*) \approx \frac{1}{5} J_d(p^*) = 90 \text{ MA/cm}^2 \quad J_d(p^*) \approx 500 \text{ MA/cm}^2$$

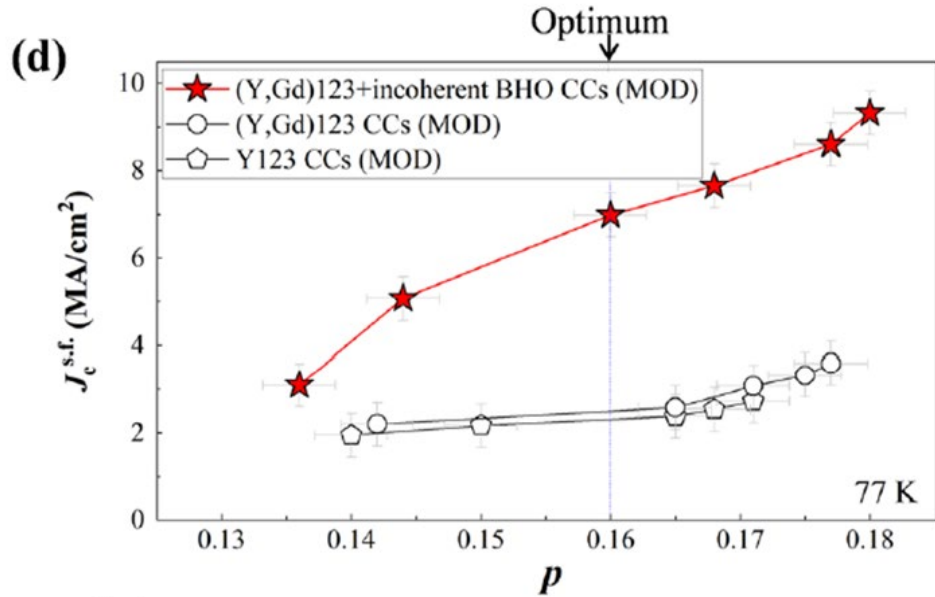
Strong increase of J_c with n_H
(x4 from p_{opt} to p^*)

$$J_c(p^{opt}) \approx \frac{1}{10} J_d(p^{opt}) \quad J_d(p^{opt}) \approx 330 \text{ MA/cm}^2$$



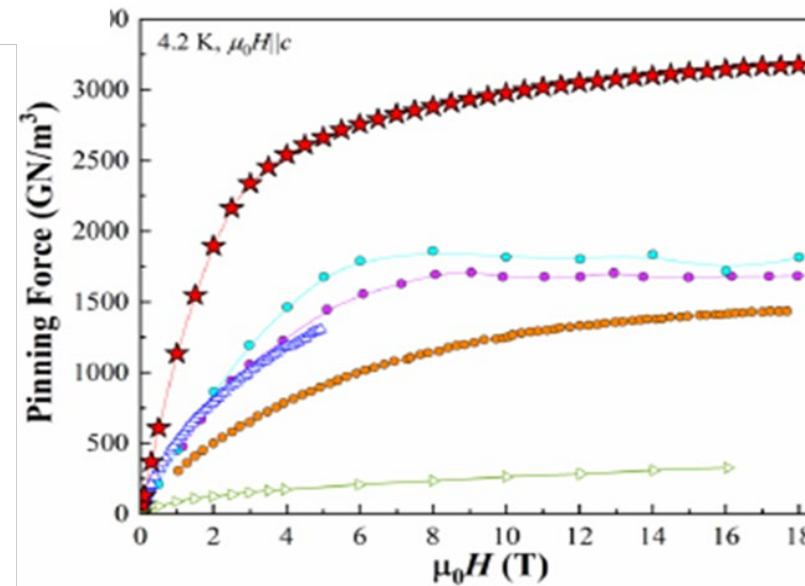
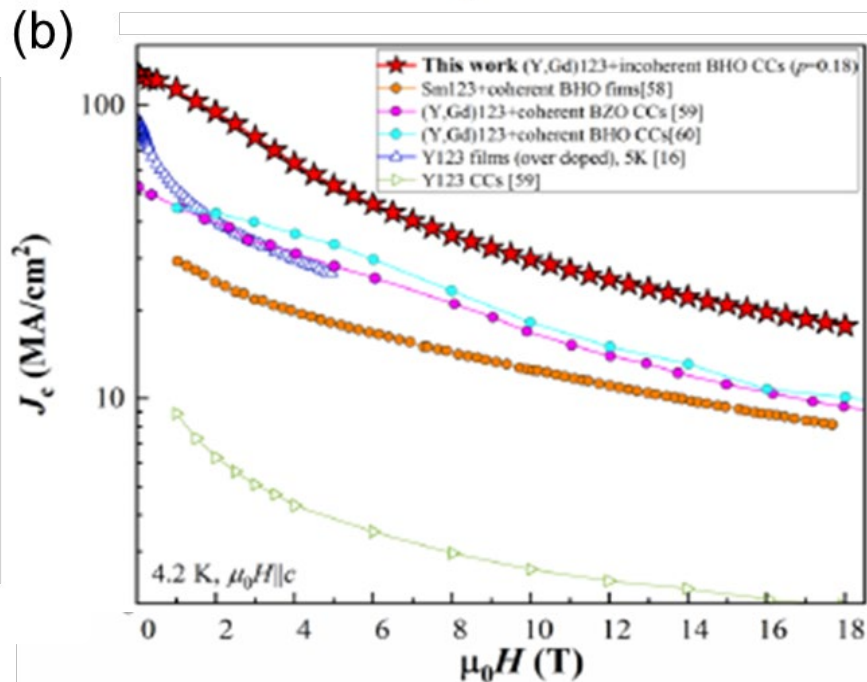
Overdoping is a robust method to reach ultrahigh $J_c(H)$

Strong increase of J_c in the overdoped state of nanocomposites



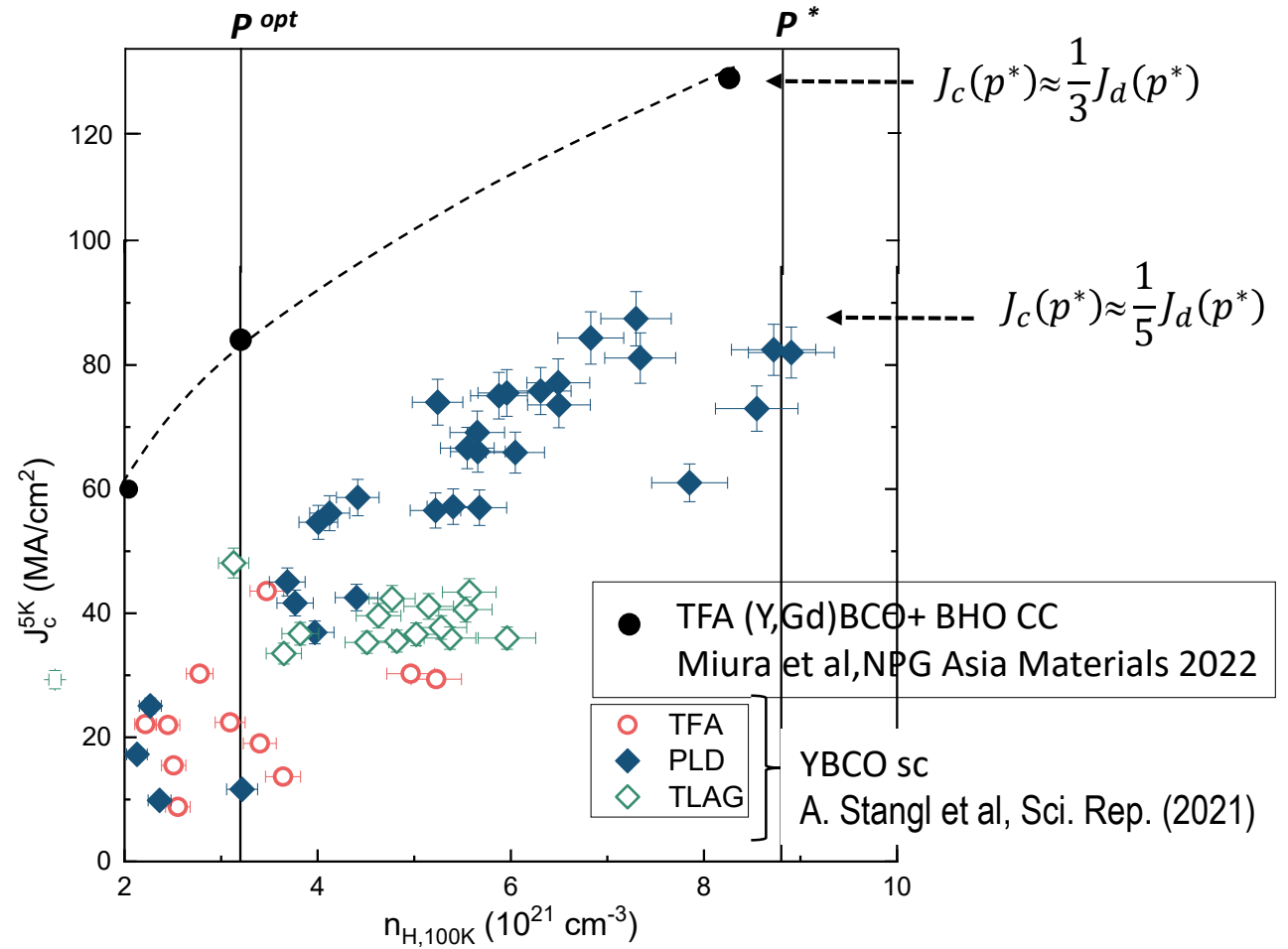
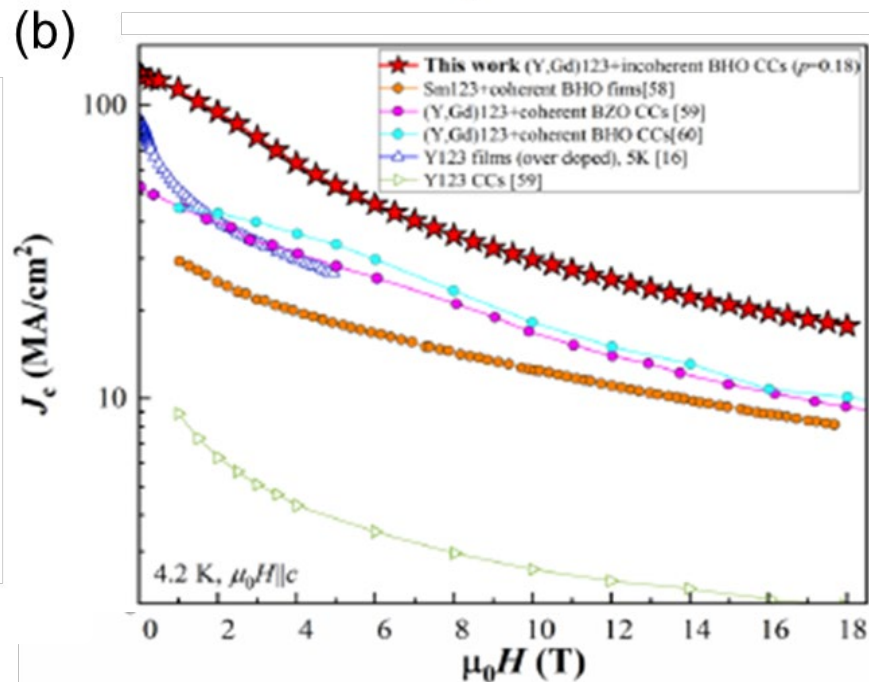
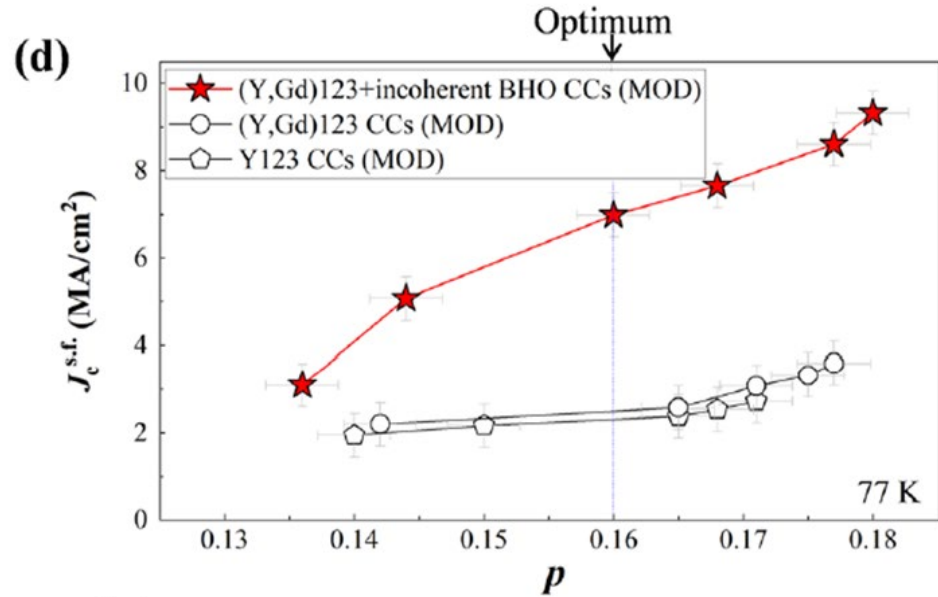
$$J_{co}^{NPS} \propto N_{np} \frac{\mu_0 H_c^2 \pi \xi^2 D}{4\xi} \propto N_{np} \left(\frac{1}{\lambda^2 \xi} \right)$$

- Nanoparticles increase of J_c^{sf}
- Influence of carrier concentration through thermodynamic parameters



M. Miura et al, NPG Asia Materials (2022)
TFA-REBCO film growth with UTOC nanoparticles

Strong increase of J_c in the overdoped state of nanocomposites



Comparison between different growth processes

Film features	Growth from vapour	Growth from liquid	Growth from solid
Growth mechanism	Gas–solid transformation	Liquid–solid transformation	Solid–solid transformation controlled by gas diffusion
Growth rate	Medium ($\approx 0.5\text{--}25\text{ nms}^{-1}$)	Ultra-fast ($\approx 100\text{--}2.000\text{ nms}^{-1}$)	Slow ($0.5\text{--}3\text{ nms}^{-1}$)
Supersaturation control	Deposition rate, T , P_{O_2}	RE ion, liquid composition, T , P_{O_2}	P_{H_2O} , T , P_{O_2}
Deposition and growth environment	Simultaneous deposition and growth: PLD, MOCVD, ME; high-vacuum environment	Sequential deposition and growth; atmospheric and intermediate pressures (TLAG-CSD); high-vacuum and intermediate pressures (RCE-DR)	Sequential deposition and growth; atmospheric pressure deposition (TFA-CSD, BaF ₂); growth at normal or slightly reduced pressures
Precursors	Targets (PLD, ME); volatile metalorganics (MOCVD)	Fluorine-free metalorganic solutions; evaporated metals (RCE-DR)	Fluorine-based metalorganic solutions (TFA-CSD); evaporated metals (BaF ₂)
Nanocomposites: second-phase nanostructures	Self-assembled nanorods, nanoparticles	Spontaneous segregation, preformed nanoparticles	Spontaneous segregation, preformed nanoparticles
Nanostructures orientation	Epitaxial	Epitaxial or random	Random
Main vortex pinning centres	Nanorods, nanoparticles, point defects	Nanostrain, nanoparticles, point defects, twin boundaries	Nanostrain, nanoparticles, point defects, twin boundaries
Critical current (A/cm-width) industrialized values	1,000–1,600 at 4.2K, 20T; 350–700 at 20K, 20T; 350–750 at 77K, 0T		
Large-scale manufacturing	Medium throughput, high CAPEX	High throughput, large areas, simplified furnaces, low CAPEX	Low throughput, complex furnaces, small areas, low CAPEX
Potential cost, performance	Medium	Low	Medium

Conclusions and take away message

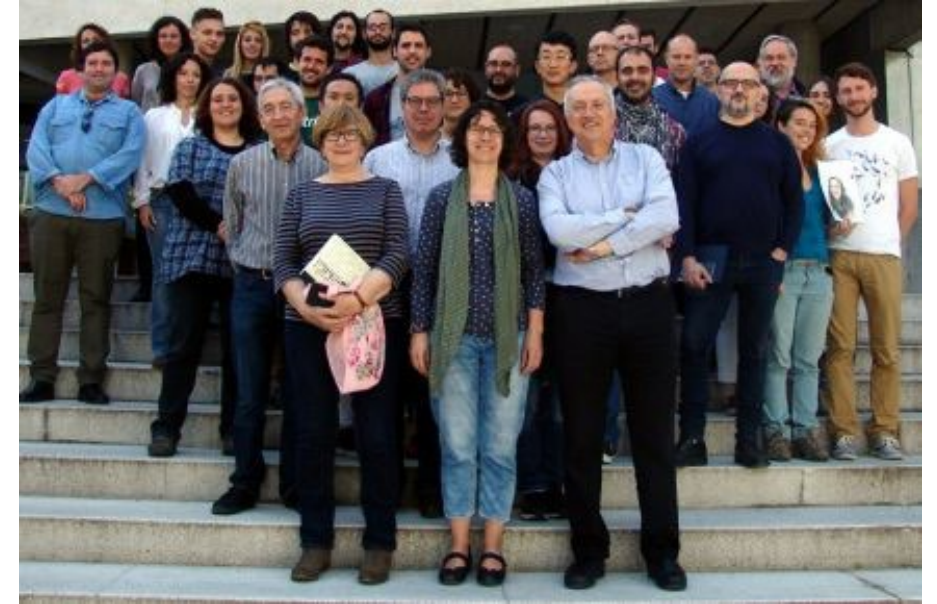


Advanced
Grant



- Coated conductors are unique superconducting materials that are set to enable UHF magnets for compact fusion
- Very long lengths of CCs are required so high throughput production is required at low cost keeping high performance
- Ultrafast REBCO growth rates are required to reduce the figure of merit cost/performance (€/kA m)
- Nanostructure deeply differs between simultaneous and sequential deposition and growth methodologies
- Reliable and fast characterization methodologies are required to identify the efficient APCs at different temperatures and magnetic fields
- Liquid assisted growth methodologies are very promising to increase throughput
- TLAG-CSD is an emerging low cost (low CAPEX-ultrafast growth) route to nanocomposite CCs with preformed nanoparticles
- We need to follow systematic studies of modifications of vortex pinning landscapes with irradiation using well established methodologies: ICMAB is open to collaborate in this challenge!

Acknowledgements



- Prof. Teresa Puig, Head Dpt.
- Members of Superconducting Materials and Large Scale Nanostructures (SUMAN) Dpt.
- Many PhDs and postdocs during the last 20 years

